10

Laser spectroscopy in medical diagnostics

S. SVANBERG, Lund University, Sweden

DOI: 10.1533/9780857097545.3.286

Abstract: Aspects of laser spectroscopy applied to the biomedical fields are reviewed with examples illustrating the techniques taken mostly from the author's research experience. Basic principles of the quantum-mechanical background are described, and powerful implementations in the biophotonics field are discussed.

Key words: optical spectroscopy, tissue optics, tissue interaction, absorption, fluorescence, Raman spectroscopy, coherent anti-Stokes Raman scattering, laser-induced break-down spectroscopy, optical coherence tomography, sub-wavelength resolution, gas in scattering media absorption spectroscopy.

10.1 Introduction to spectroscopy

Spectroscopy is the science of elucidating energy level structures in physical systems, ranging from atoms to solid-state aggregates. Quantum mechanics is able to explain such structures with various degrees of precision depending on the complexity of the system. The origin of quantization in physical systems relates to the fact that the fundamental particles, generally electrons, building up the easily observable parts of the system have a wave nature, and thus are subject to constructive and destructive interference. There is a parallel with the guitar string, which supports a fixed frequency (and overtones) while all other frequencies – possibly tried by the string! – will be eliminated by destructive interference. Mostly, energy levels are not observed directly, but rather the difference in energy ΔE between levels $E_2 - E_1$, revealed by measuring the energy of the radiation necessary for inducing a transition between a lower and the upper state (photon absorption), or the energy of the radiation quantum emitted when the system returns to the lower state (photon emission), normally after a short time, ranging from picoseconds to milliseconds. According to Planck and Einstein, we have

$$\Delta E = E_2 - E_1 = h\nu = h\frac{c_0}{\lambda} \qquad [10.1]$$

where ν is the frequency of the light, h is Planck's constant, c_0 is the velocity of light, and λ is the wavelength.

Spectroscopy deals with the experimental determination of the energy, frequency or wavelength of the radiation observed in the transition process. Frequently, the wavelength of the light is measured in spectrometers, where the

wave nature of the emitted quanta is explored, again in constructive or destructive interference. This is the case in prism, grating, Fabry-Perót or Michelson spectrometers/interferometers, which are common when analyzing radiation in the ultraviolet (UV), visible, or infrared (IR) parts of the spectrum. Other spectrometers directly detect the energy deposited when a discrete quantum is absorbed. Frequently, such systems are used for higher quantum energies, such as in the X-ray or gamma-ray spectral regions. Long-wavelength photons of low energy, i.e. radio or microwaves, use further technologies, well known from the classical telecommunications field.

Medical spectroscopy employs electromagnetic waves in wide wavelength ranges, ranging from radiofrequency (magnetic resonance imaging, MRI) to X-rays and gamma-rays (conventional X-ray imaging and computerized tomographic (CT) X-ray imaging. In between we find the UV, visible and IR regions where lasers work. We will focus on laser spectroscopy in the present chapter, meaning that we will restrict ourselves to this intermediate energy range of the electromagnetic spectrum.

Sometimes differences in energy between levels can be elucidated by studying the temporal behavior of the light emission following coherent excitation of both levels with a short pulse, energetically overlapping both levels. In the decay of the coherently excited levels there will be intensity beats in the emission with frequencies corresponding to energy level spacings. The energy level structure can then be elucidated by Fourier transforming the temporal structure, yielding the frequencies responsible for the interference pattern observed. This is called quantum-beat spectroscopy. Generally speaking, observing the temporal evolution of the emission following abrupt excitation of energy levels will reveal the dynamics of the system. We include studies in the temporal domain within the concept of spectroscopy.

Spectroscopy in different energy ranges is discussed in monographs on the topic, e.g. Svanberg,[1] Thorne *et al.*[2] and Banwell and McCash.[3]

10.2 Energy levels in atoms, molecules and solid-state materials

10.2.1 Atoms

Most of the about 90 more or less stable elements in the periodic system are of some interest in medicine, sometimes as key constituents of human tissue, sometimes as dangerous pollutants. Free atoms are extremely seldom encountered in biological contexts, where atoms join into free molecules (physiological gases) or into condensed matter or tissue in the common sense, making up muscles, fat and body liquids.

Atoms, being the most fundamental building bricks of the world we observe on an everyday basis, are built up with negatively charged electrons arranged

in shells around a positively charged nucleus, exactly balancing the net charge to zero. The existence of a periodic system, where chemical and physical properties regularly repeat themselves, e.g. in the group of alkali atoms, halogens or inert gases, is due to the existence of 'closed' shells of electrons which normally do not engage in energetic excursions. Instead, electrons outside closed shells are active in transitions generating spectra to be studied by the spectroscopist. If elements have a similar electronic structure outside closed shells they became similar in their general behavior, explaining the periodicity.

The inert gases have no electrons outside closed shells and remain chemically passive. They do not form molecules. The atmosphere contains small amounts of such gases, e.g. helium, argon and xenon. On inhalation they remain inert. Recently, spin-oriented helium and xenon have found interesting medical applications in MRI of lungs, enabling powerful mapping of the lung tree.[4,5] Mercury, as an exception among the other atoms, is present as a serious air pollutant in atomic form, and has been much studied (see, e.g., Mazzolai *et al*.,[6] Svanberg[7] and Grönlund *et al.*[8]). The ability of mercury to transform into methyl mercury makes it a special concern among heavy metal pollutants.

As a model for simple atoms we could take sodium, for which the single electron outside closed shells containing 10 electrons makes energy jumps and thereby generates the absorption or emission spectrum of sodium. The most prominent sharp line corresponding to an electron jumping from the first excited state to the ground state is the yellow line at 589 nm, well known from the common sodium lamps. As mentioned, we could instead focus on the energy of the quantum, normally expressed in electron volts (eV). We note that 600 nm corresponds to 2.0 eV, meaning that UV light at 300 nm corresponds to 4.0 eV, and IR transitions around 10 micrometers correspond to about 0.12 eV.

10.2.2 Molecules

Atoms form molecules, and the driving force for this is that they can minimize their total energy in this way. The simplest molecules are the diatomics, such as H_2, hydrogen, O_2, oxygen or N_2, nitrogen. As with atoms, outer common electrons can be excited or de-excited, normally leading to characteristic spectra in the visible or UV regions. Molecules also exhibit further structures due to their ability to vibrate (periodic stretching of the bond interconnecting the atoms) and to rotate. Again, these motions are subject to quantization and the corresponding spectra typically fall in the IR spectral region, and in the radio (meter waves) or microwave region (mm waves), for the case of vibrational and rotational transitions, respectively. In practice, all three types of energy jumps occur at the same time, leading to complex but characteristic spectra. The diatomics are reasonably simple, while polyatomic molecules exhibit very complex spectra. Among physiological gases of particular relevance in medicine, we will especially

encounter the diatomics oxygen and nitrogen and the triatomics water vapor, H_2O, and carbon dioxide, CO_2. These gases are used in medical applications of gas in scattering media absorption spectroscopy (GASMAS),[9] which we will discuss further below. Other gases, including nitric oxide, NO, formaldehyde, HCHO, and ethylene, C_2H_2, are of clinical relevance because their presence in exhaled gas may signal important diseases such as diabetes, renal failure, etc. Multipass absorption cells or cavity ring-down spectroscopy is used to achieve sufficient sensitivity for such trace gases (for an account of spectroscopic breath analysis see, e.g., Wang and Sahay[10]).

10.2.3 Condensed matter

Human tissue contains a lot of water (more than half of the body weight is typically water), lipids, and proteins. The strongly colored hemoglobin is of particular interest regarding spectroscopic studies of human tissue. When atoms and molecules form liquid or solid substances, rather broad energy bands occur instead of the sharp energy levels of free atoms and molecules. This is due to the strong perturbations which the individual constituents exert on each other. Broad energy bands correspond to broad absorption and emission bands. This means that the need for a high spectroscopic resolution in studying human tissue is not needed, normally making the equipment simpler. However, on the negative side, the broad structures clearly often overlap, making it difficult to discern individual constituents in a complex material such as human tissue. We will deal with this problem later.

Very schematic energy level diagrams for atoms, molecules and condensed matter are given in Fig. 10.1.

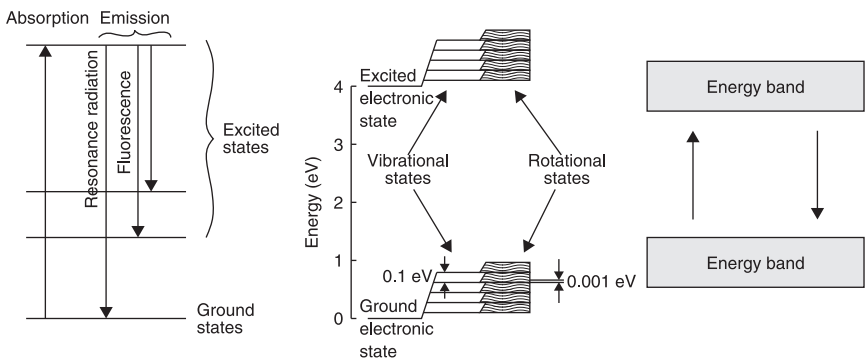

10.1 Schematic energy level structures for atoms, molecules and condensed matter, and radiative transitions (from Svanberg[1]).

10.3 Radiation processes

We will now briefly describe different radiation processes governing the interaction between matter and electromagnetic radiation. Basically, we distinguish between resonance radiation, where the absorbed or emitted quanta energetically correspond exactly to the energy level difference, according to Eq. 10.1, and scattering processes, where such a match is absent.

10.3.1 Dipole radiation

Easily observed transitions between energy levels as described by Eq. 10.1 occur due to what is referred to as electric dipole interaction. Quanta absorbed or emitted exactly balance up for the energy difference between the levels involved. Actually, this so-called resonance condition is necessary for the transition to occur, but not sufficient. Due to the quantum nature of the system studied, energy levels described by proper wavefunctions have symmetry properties which must have a specific relationship to allow the transition (parity considerations).

Absorption

In absorption processes, impinging radiation is absorbed and the system is energetically raised to an excited state. The process is manifested in a reduction of the intensity of radiation flux after passing through a sample of atomic or molecular constituents, as illustrated in Fig 10.2(a). Recording of an absorption spectrum requires a broadband emission source, as indicated in the figure, out of which certain characteristic wavelengths are reduced in intensity when the resonance condition is fulfilled. A spectrometer is needed to sort the absorbed wavelengths from those not absorbed. Planck radiators or electron synchrotrons are used as radiation sources in absorption experiments. With the advent of tunable lasers, a single but more or less widely tunable wavelength is generated. The beam is attenuated by the sample when tuned through the resonances of the sample. Here the tunable laser plays the role of both radiation source and spectrometer, eliminating the need for the latter. Lasers of different types are discussed in standard monographs on the topic (see, e.g., Svanberg[1], Chapter 8); Svelto[11]).

Emission

An excited state is basically short-lived, since there is an inherent tendency in nature to attain as low energy as possible. Excitation may have been incurred by absorption of appropriate light quanta or by electron impact. On decay, a photon is emitted, making up for the energy loss. The energy of the quantum can be

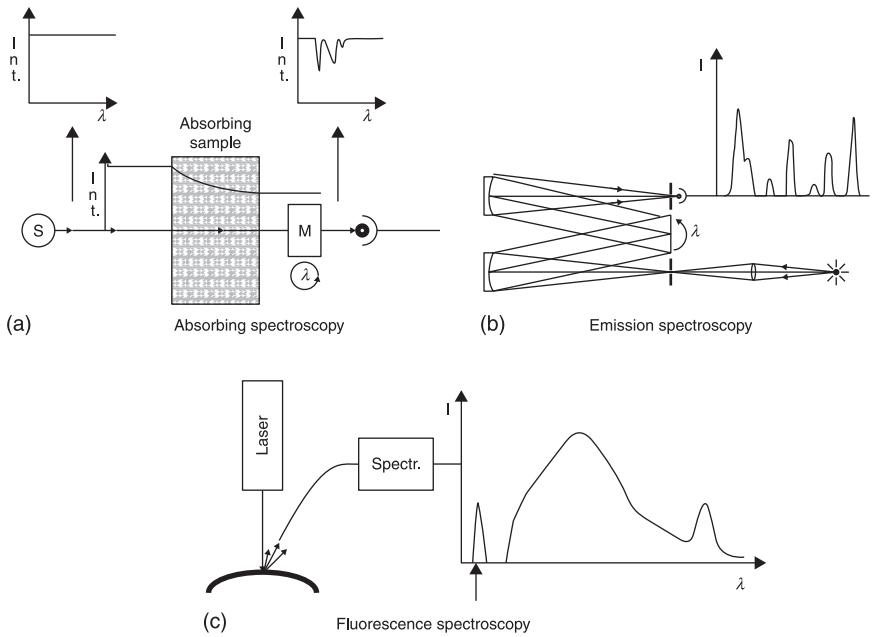

10.2 (a) Absorption measurements, (b) emission measurements, (c) fluorescence measurements.

assessed by a spectrometer, which would record an emission spectrum. We note that an emission spectrum starts from zero and rises to intensities corresponding to the individual emission lines (Fig. 10.2(b)). In contrast, absorption spectra correspond to a reduction in a strong background intensity – thus small absorptions are difficult to discern.

For molecules and condensed matter there are many possible energy levels, and complex absorption and emission spectra occur. In condensed matter, many different excitation wavelengths are possible. Due to interactions, molecules in different sublevels of the excited state will relax down to the lower level of the electronically excited state, from which transitions to a multitude of lower sublevels of the lower electronic state can occur. Then a broad distribution of radiation, a fluorescence spectrum, will be observed, always shifted towards the low-energy direction (longer wavelengths) with regard to the excitation wavelengths (see Fig. 10.2(c)). The fluorescence spectrum carries information on the structure of the lower state. Because of the interactions between the constituents of condensed matter, most of the excited molecules return to the ground state due to collisional relaxation, not yielding light emission but leading to heating of the sample. This effect can be utilized in photoacoustic spectroscopy of tissue, to be discussed below.

The origin of linewidth

In spectroscopy there is frequently a quest to achieve spectral resolution as high as possible in order to accurately determine the position of energy levels and to be able to distinguish the spectral imprints from various atoms, molecules and aggregates. We may, then, ask ourselves what is the limit of spectral resolution. Clearly, the resolving power of the spectrometer or laser employed is very important, but here we focus, rather, on the more fundamental limitations imposed by the system studied. The fact that an excited state has a limited lifetime, as discussed above, leads to a fundamental uncertainty in energy assessment due to the limited time to perform the measurement task (the Heisenberg uncertainty relation). The natural radiation width of the transition due to this fact is always negligible in biomedical spectroscopy.

Free gases at atmospheric pressure exhibit considerable line broadening in practice, for two reasons. One is the fact that the particles are moving, with a velocity distribution with typical spreads of few hundreds of m/s and in all directions. This gives rise to a Doppler broadening. According to the Doppler formula, light at frequency ν will be subject to a Doppler shift $\Delta\nu$

$$\frac{\Delta\nu}{\nu} = \frac{v}{c} \qquad [10.2]$$

where v is the velocity of the particle along the line of sight and c is the velocity of light (3×10^8 m/s). We note that v/c has a typical value of 10^{-6}, transferred to an uncertainty in the sixth digit of the transition frequency and thus in the wavelength. At low pressures this Doppler broadening determines the observed sharpness of the spectral line.

Frequent collisions between free gas molecules at atmospheric pressure force them to collisionally return to the ground state without emitting radiation (*quenching*). The upper state lifetime is then shortened by several orders of magnitude, making the corresponding broadening comparable to or even larger than the Doppler broadening. Due to the different types of interaction, the corresponding line shapes are different, *Lorentzian* for collisional and *Gaussian* for Doppler broadening (mathematically of type $1/(1 + x^2)$ and $\exp(-x^2)$, respectively). In practice a convolution of these lineshapes, a *Voigt* curve, is observed, and an uncertainty in the fifth or sixth significant figure of the wavelength or frequency results. In GASMAS or exhaled gas monitoring such lineshapes are observed.

As mentioned above, for condensed matter, such as human tissue, spectroscopic structures observed are much broader due to the occurrence of broad energy bands in such materials. Thus the requirements for spectroscopic resolution are normally quite modest in tissue spectroscopy, where information beyond a second or a third significant digit in the wavelength assignments is not present.

10.3.2 Scattering

Scattering occurs even when the resonance condition between photon energy and energy level separation occurs. Some of the incoming photons are scattered in different directions upon interaction with the surrounding matter. If the wavelength is unaltered we talk about *elastic* scattering; if a change occurs the process is characterized as *inelastic*. Scattering processes are orders of magnitude weaker than electric dipole transitions.

Elastic scattering

This type of scattering is denoted to be of *Rayleigh* type if the scattering occurs on particles of size much smaller than the wavelength of the incoming light, and of *Mie* type if the contrary is true. Both types of scattering have a strong wavelength dependence (proportional to $1/\lambda^4$ and about $1/\lambda^2$, respectively). This wavelength dependence explains, e.g., why the clear sky is blue and sunsets are red. Scattering is illustrated in Fig. 10.3(a).

Inelastic scattering

Wavelength shifts occur in scattering for basically two different reasons. The first reason is the same as already encountered in Section 10.3.1; the *Doppler effect*. In biological tissue the motion of relevance is the flow of blood, especially the capillary blood flow. Since typical velocities of the red blood cells in capillaries are a few mm/s, the v/c ratio in Eq. 10.2 becomes 10^{-11}. For visible light with a frequency of about 10^{14} Hz the resulting minute shifts will be in the kHz region and only detectable using *heterodyne* techniques whereby the shifted and unshifted light components interfere on the detector, resulting in a beat frequency reflecting

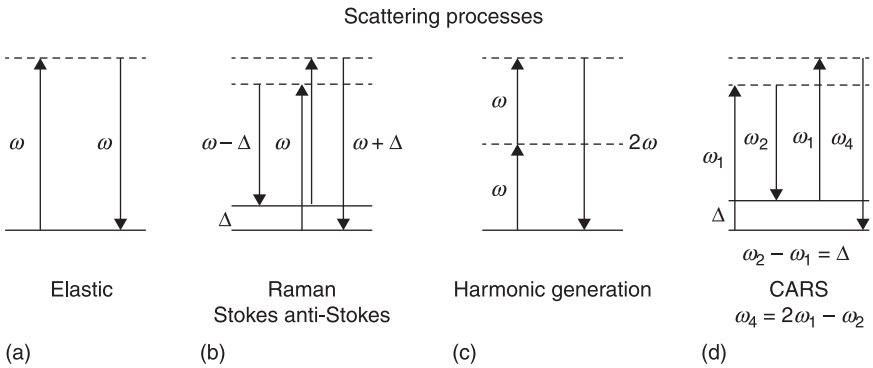

10.3 (a) Elastic scattering, (b) Raman scattering, (c) second harmonic generation, (d) Coherent anti-Stokes Raman Scattering (CARS).

the blood flow. Considering also the strength of the shifted signals, which is proportional to the number of moving particles, the *perfusion* of the tissue can be assessed.

Substantially larger shifts of a completely different origin occur through the interaction of the incoming light field and the molecular vibrations. When a system is driven at two different frequencies simultaneously (optically and vibrationally) a coupling occurs, leading to the sum and difference frequencies also being weakly generated. These components, shifted upwards and downwards in frequency with respect to the driving field (the carrier), are denoted the *anti-Stokes and Stokes Raman components*, respectively. This is illustrated in Fig. 10.3(b). Raman signals are very weak, and strong laser radiation is needed for their observation.

The signals can be enhanced by tuning the carrier frequency close to a resonance – *resonance Raman spectroscopy*. Strong enhancements in intensity can also be obtained *through plasmon resonances* at silver and gold particle surfaces, giving rise to *surface enhanced Raman scattering* (SERS). Using high-intensity laser beams, *stimulated Raman scattering* (SRS) can be induced as well as *second-harmonic generation* (SHG) (Fig. 10.3(c)) and *coherent anti-Stokes Raman scattering* (CARS) (Fig. 10.3(d)). The three latter processes are non-linear and coherent, meaning that the generated signal emanates as a coherent laser-like beam (see, e.g., Svanberg,[1] Chapter 8). For stimulated Raman scattering the beam has the normal Raman wavelength. In the SHG process, two photons are converted into one new photon with double energy, i.e. double frequency or half the wavelength. In CARS, one first pump photon beam combines with one Stoke-shifted laser beam to coherently drive a vibration in the lower state where the difference frequency between the two laser beams corresponds to the vibrational frequency. Then a further pump photon combines with the driven vibration to generate a new anti-Stokes signal beam, with a frequency higher than any of the incident laser beams. Thus, the signal occurs at a wavelength where there is no laser-induced fluorescence, which always occurs on the Stokes side. Coherent processes are increasingly being utilized in many novel types of tissue microscopic imaging.

10.4 Absorption and emission spectra

We will give first examples of tissue absorption and emission spectra in this section. The spectral shapes are useful in identifying different substances in the tissue – as mentioned, this is not always an easy task, since the spectral features are broad and overlapping. Apart from species identification, quantification of the constituents is of considerable interest. Basically, the emission light intensity in incoherent processes is within certain limits proportional to the number of molecules participating in the process. For absorption, the observed attenuation is related to the concentration through the *Beer-Lambertian law,* which is illustrated

in Fig. 10.2(a). The law states that the intensity I(x) of the light falls exponentially through a non-scattering medium from its initial value I(0) with the attenuation governed by the product of the concentration c, the distance traveled x and a molecular-specific factor k, which is determined by quantum mechanics. Thus,

$$\frac{I(x)}{I(0)} = e^{-kcx} \qquad [10.3]$$

By taking the logarithm of this expression the concentration can be obtained if the layer thickness x is known, which is the case in a non-scattering medium. While in principle the constant k could be calculated from quantum mechanics, it is in practice determined through calibration with known concentrations. As we will see below, a complication in the case of tissue is that strong scattering makes the distance *x* in Eq. 10.3 undefined. Since the product of *c* and *x* is measured, it will mean that the concentration is also undefined. We will discuss how this problem can be tackled.

10.4.1 Absorption spectrum of tissue: tissue optical window

Any discussion of applications of optics or lasers in medicine must start with a thorough consideration of the absorption properties of the main constituents of tissue. Water has a very strong absorption at short UV wavelengths and again at wavelengths longer than 1.4 μm, with particularly strong absorption peaks at 1.9 and 3.0 μm. Proteins strongly absorb through the UV region below about 400 nm, while the melanin pigment in the skin has a broad absorption from the UV with successively weaker attenuation through the visible region. Of particular importance is the chromophore hemoglobin, whose red color derives from the fact that it massively absorbs below 600 nm but is largely transparent to red color (wavelengths longer than 600 nm). The net effect of these major chromophores results in a region above 600 nm and below 1.4 μm where the human body is relatively transparent, meaning that optical radiation can penetrate distances ranging from a millimeter to several centimeters, depending on the exact wavelength. We refer to this region as the *tissue optical window*. The absorption spectrum of human tissue is discussed in detail in Boulnois.[12] An important group of mostly artificial chromophores are sensitizers, which can be used for inducing photodynamic therapy processes utilized in malignant tumor abatement, or for tumor demarcation. To be efficient they should have absorption bands within the tissue optical window to allow the processes to take place at deeper levels, not just at the surface.

10.4.2 Emission spectra from tissue

Light can emerge from tissue at wavelengths different from the incident one due to several spectroscopic interactions. The most important ones are fluorescence, laser-induced breakdown emission and Raman scattering.

Fluorescence spectroscopy

According to Section 10.3.1, red-shifted (Stokes shifted) fluorescence emerges from tissue subject to radiation at shorter wavelengths, normally in the blue or UV spectral regions. The distribution of *laser-induced fluorescence* (LIF) frequently shows rather little structure due to the action of several constituents, most of which have broad emission spectra. Sensitizers frequently have sharper features (typically with peaks of 20 nm half-width), making their presence more easily discernible. By changing the excitation wavelength, different constituents, absorbing differently as a function of wavelength, will be weighted differently in the resulting fluorescence spectrum, which adds to the possibility of distinguishing different tissue types. Porphyrin sensitizers have maximum absorption around 405 nm (the *Soret* band); such a laser wavelength will thus enhance sensitizer fluorescence. The fluorescence from endogenous chromophores is more prominently excited at lower wavelengths. Figure 10.4 illustrates these aspects – a fluorosensor with three optional excitation wavelengths derived for light-emitting diodes (LEDs) is being employed.[13]

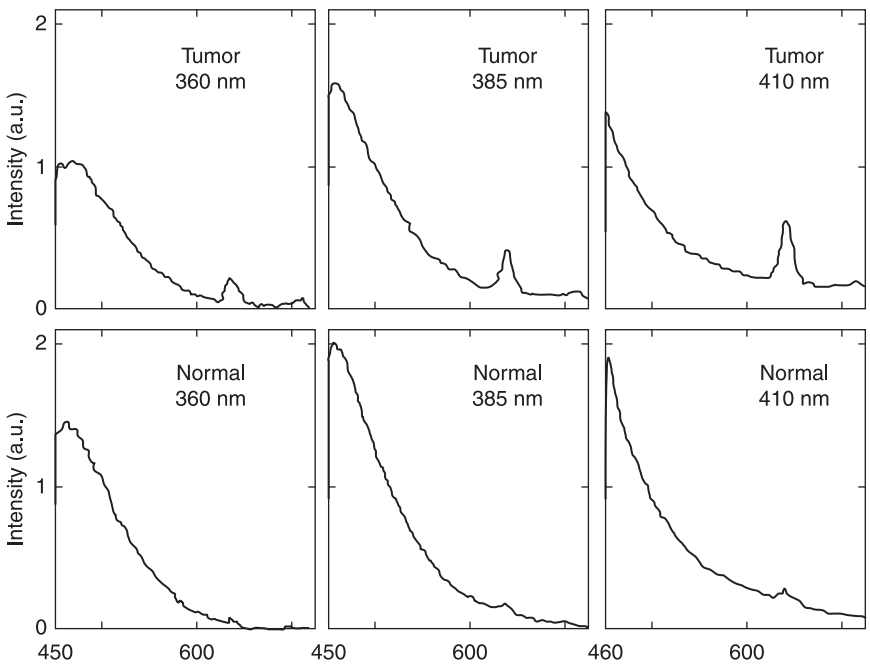

10.4 Laser-induced fluorescence spectra recorded for two tissue types irradiatated at three different wavelengths. Selective retention of a sensitizer in tumor tissue is observed, and also that the sensitizer is relatively better excited by 410 nm then at the shorter wavelengths (from Ek *et al.*[13]).

Raman spectroscopy

In contrast to fluorescence spectra, those induced by the Raman process feature comparatively sharp peaks due to molecular vibrations, which are normally observed on the Stokes side of the carrier (Stokes–Raman components). A complication is that the normally much stronger LIF process induces a broadband background in which the Raman peaks occur. We will discuss how to abate this problem below in Section 10.8.1. A basic observation is that it is necessary to strongly suppress the much stronger peak due to the elastically scattered irradiating light (the Rayleigh/Mie component). This can be achieved with double monochromators and/or the use of notch filters, strongly suppressing the carrier but letting close-lying radiation through efficiently.

Laser-induced breakdown spectroscopy (LIBS)

Sufficiently strong and focused beams from pulsed lasers give rise to a hot plasma formation, and the plasma becomes a source for *laser-induced breakdown spectroscopy* (LIBS). In contrast to LIF and Raman, in which the emission comes from molecules, free atoms and ions in the plasma radiate characteristic sharp lines directly carrying information on the atomic constituents. Initially a broad light distribution from the hot plasma is observed, but in the cooling plasma the background light is fading away and sharp emission lines are observed in the after-glow.

The LIBS technique in medicine has applications regarding control of laser lithotripsy of kidney and gall bladder stones, in which acoustic shockwaves force the stones to disintegrate after being subjected to pulsed laser radiation through a fiber inserted through the relevant ducts. The LIBS spectrum can reveal the composition of the stone and guide pulse energy settings. This concept is illustrated in Fig. 10.5. It can also have applications in guiding laser angioplasty, where atherosclerotic plaques in the carotids are cleared using similar techniques.

10.5 Interplay between absorption and scattering in turbid media

Biological tissue is strongly scattering for optical radiation. This fact leads to two major problems in the application of laser techniques in biomedicine. 1) The scattering results in the optical pathlength through the medium investigated being undefined – part of the light travels shorter distances, part substantially longer distances. Thus, the Beer-Lambert law as stated in Eq. 10.3 is no longer valid. 2) The strong multiple scattering leads to blurring of images taken through tissue layers.

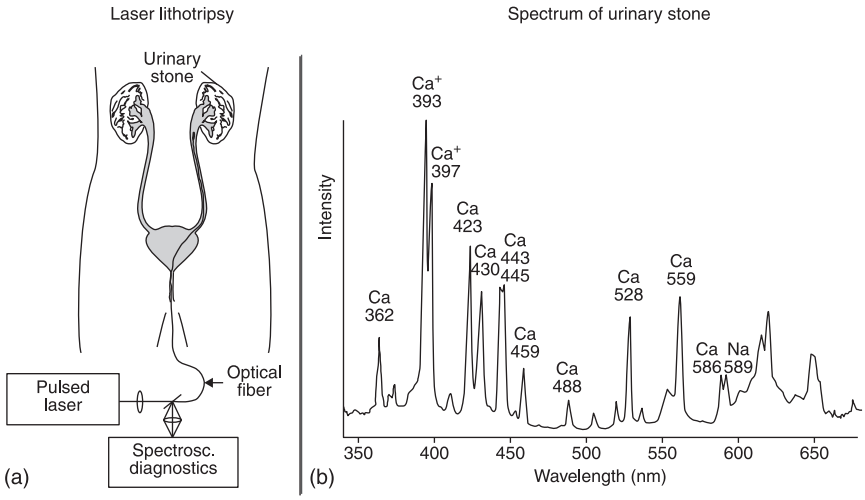

10.5 Illustration of laser-induced breakdown spectroscopy (LIBS) in connection with laser lithotripsy of kidney stones (from Andersson-Engels *et al.*[14]).

In analytical chemistry the turbidity of a sample, i.e. a pharmaceutical preparation, leads to difficulties in a direct assessment of drug constituent concentrations because of the scattering. Classical spectroscopic measurements are therefore combined with multivariate techniques, which, after calibration with known samples, still provide possibilities for quantitative analysis.[15]

Using time-resolved spectroscopy, it is possible to decouple absorption from scattering. When short, picosecond or femtosecond pulses are launched into tissue, the light emerges after multiple scattering at different time delays at a detector placed at some distance from the light injection point. Due to multiple scattering, some photons arrive late at the detector. In the case of substantial absorption, the tail is largely suppressed because the chance of absorption is substantial. While the shape of the whole curve can be understood in detail from the transport equation,[16] it can be intuitively understood that the slope of the late tail is largely determined by the absorption, while the width and peak position of the distribution are largely determined by the scattering. By a detailed fit of the experimentally determined shape and theoretical distributions for varying absorption and scattering coefficients, absorption can be determined as if scattering were absent, and scattering can be determined as if absorption were absent. By using white light illumination from a femtosecond self-phase modulated source and crossing a spectrometer with a streak camera, wavelength-dependent values of the absorption and the scattering coefficients can be experimentally determined as a function of wavelength.[17]

As an alternative, launching light into a medium and detecting emerging light at successively increasing distance from the injection site can yield separate information on absorption and scattering; however, only when certain assumptions are fulfilled.[18] Further, it was noted by Bigio *et al.* that, for a particular 'magic' separation between injection and detection points, absorption data become largely independent of scattering,[19] making the construction of relatively simple tissue diagnostic probes possible.

10.6 Absorption and scattering spectroscopy of tissue

10.6.1 Spectroscopic considerations in laser therapy

The absorption properties of the main tissue chromophores, as discussed in Section 10.4.1, strongly govern the thermal and ablative interactions between laser radiation and human tissue. Surgical use was the first application of lasers in medicine. Using CW lasers, the interaction is governed by heat generated following absorption of photons. Tissue coagulates around 60 degrees and carbonizes above 200 degrees. Spectroscopic aspects, i.e. the interaction as a function of the laser wavelength used, relate to the strength of the absorption and thus the penetration depth of the radiation. Carbon dioxide laser light around 10 microns has very shallow penetration, and thus the heat is very localized, leading to quite a sharp transition from affected to non-affected regions of the tissue. Around 2 μm there is a distinct strong absorption peak of water; the Holmium YAG laser at 2.1 μm is very suitable for certain surgical interventions. The Nd:YAG laser at 1.06 μm penetrates much further and the heat is distributed, leading to a thicker coagulation zone with advantages for hemostasis of blood vessels. Tuning a yellow dye laser to 580 nm takes advantage of the strong hemoglobin absorption peak in a wavelength region where proteins, etc., show little absorption. The selective action of blood heating on port-wine stains and telangiectasia leads to particularly good results on superficial blood vessel anomalies. Moving towards short wavelengths, an increasing absorption of proteins leads to very shallow penetration depths. Using short-pulse lasers in the nano- to femtosecond regime leads to much energy deposition in a very shallow region followed by explosive expansion of the generated hot plasma. Cell layer by cell layer can be removed in precision surgery, required for corneal resculpturing for focal length engineering to remove the need to wear glasses. Short-wavelength lasers, such as excimer lasers, also have potential for laser ablation of *atherosclerotic plaques*, e.g. in the carotids. Spectroscopic guiding based on fluorescence or LIBS is then essential to ensure a safe procedure. Laser angioplasty with spectroscopic control is illustrated in Fig. 10.6.[20] Thermal and ablative actions of lasers are discussed, e.g., in Pettit and Waynant.[21]

Tumor-seeking sensitizers can be activated by laser light, leading to necrosis of tissue, primarily due to the release of singlet oxygen preferentially in tumors. The

process is referred to as *photodynamic therapy* (PDT).[22] Clearly, it is desirable to have a good light penetration into the tissue to be able to treat thicker tumors. Thus, the sensitizers should have a sizable absorption within the tissue optical window. Direct surface irradiation is possible for treating common skin lesions such as basal cell carcinoma or squamous cell carcinoma. Here the use of topical distribution of delta-amino levulinic acid (ALA) on the lesion followed by its selective conversion into the sensitizer Protoporphyrin IX (PpIX) has been particularly successful and is now routinely used in dermatology.[23–25] Deeper and large lesions require light administration through optical fibers inserted into the tumor mass (*interstitial PDT*). Optimal results are obtainable only when using integrated dosimetry, preferably using the same optical fibers.[26,27] Monitoring of

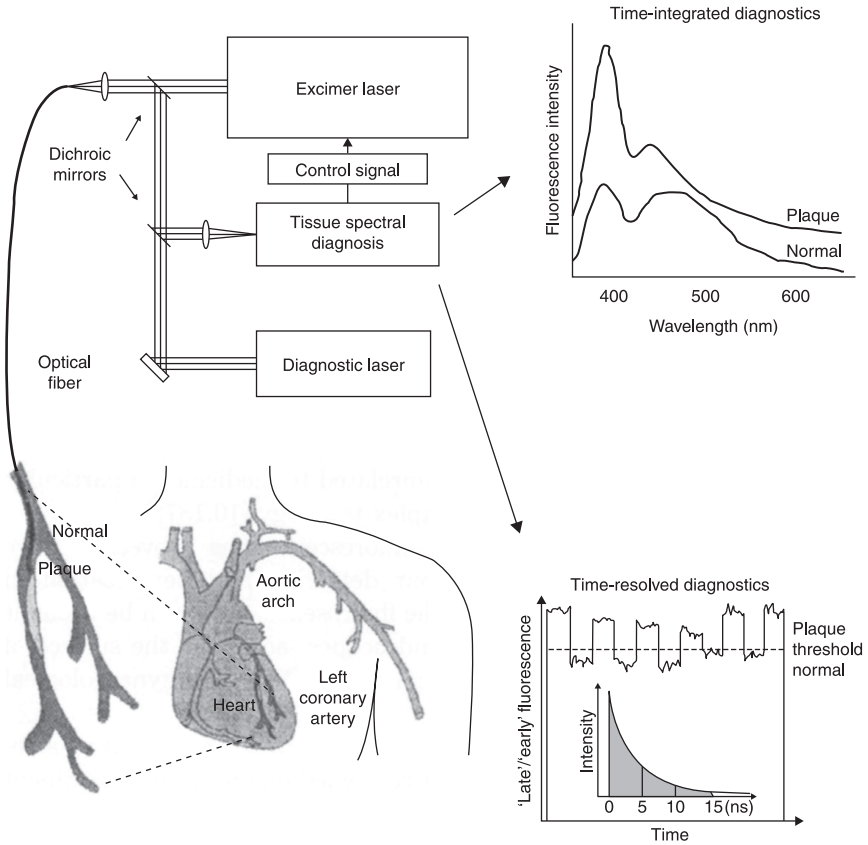

10.6 Illustration of laser angioplasty with spectroscopic guidance. A weak laser induces fluorescence in the aortic wall, which is evaluated in the spectral and time domains. If an algorithm based on the spectroscopic finding indicates that atherosclerotic plaque is in front of the fiber tip, a high energy pulse is fired. The process continues till the vessel is cleared of atherosclerotic plaque (from Svanberg[20]).

the three quantities of importance in PDT – light flux/dose, sensitizer concentration, and tissue oxygenation – should be performed. Interstitial PDT shows substantial promise for many malignant tumor types, e.g. prostate cancer, pancreatic cancer, breast cancer and brain tumors such as glioma. General accounts of the field of PDT are given, e.g., in Zeitouni *et al.*[28] and Huang.[29]

10.6.2 Tissue oxygenation

Spectroscopic considerations entered early into laser medicine through the advent of optical real-time measurements of tissue oxygenation. The techniques rely on the fact that in the near-IR spectral region, part of the tissue optical window, the residual absorption depends on hemoglobin. However, oxygenated hemoglobin and deoxygenated hemoglobin absorb differently in certain spectral regions, while they absorb equally at a therefore suitable reference point, around 805 nm, *the isobestic point.* Thus, by comparing the intensities of transmitted light through a finger tip at this point and, e.g., around 900 nm (*pulse oximetry*), it is possible to determine the oxygen saturation of tissue.[30] Sometimes the two wavelengths are instead chosen at 660 and 940 nm. The technique is much used in patient surveillance, e.g. in connection with surgery. More general near-infrared spectroscopy (NIRS) and *tissue viability imaging* (TVI) are techniques to further assess blood dynamics, e.g. blood volume, etc.

Oxygenation studies are well complemented by laser Doppler measurements of blood flow, as discussed in Section 10.3.1. Imaging instruments have recently been developed using whisk-broom scanning (i.e. collecting data sequentially point by point and line by line) of a laser beam across the area to be studied. The beat frequency spectrum and its intensity, which is dependent on the blood corpuscle movement speed and number, are evaluated with spatial resolution.[31,32] Monitoring of wound healing and possible complications related to transplanted tissue are examples of fields where perfusion imaging is of great value. A comparison of NIRS, TVI and Doppler perfusion techniques was recently made in Krite Svanberg *et al.*[33]

10.6.3 Measurements on embedded chromophores, tomography

As we have already noted above, spectroscopy and imaging in scattering media present many challenges. Early work on mapping out the oxygenation in deep-lying tissue, such as in the brain, explored time domain techniques as well as CW approaches.[34] Applications include detection of bleeding in the brain after trauma to the skull, and oxygenation assessment in the brains of newborns.[35] A further aspect is to access the true concentration and uptake contrast between malignant tumor and surrounding healthy tissue. Correct absorption measurements avoid interpretation problems when relying on fluorescence intensity measurement of

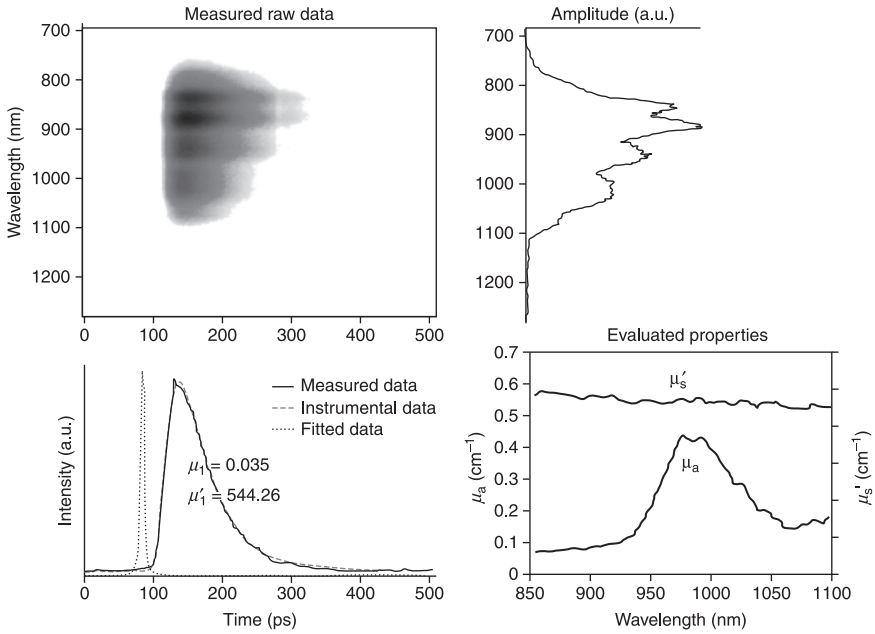

10.7 Measurement of the true absorption and scattering properties of a sample containing water. Simultaneous temporal and spectral recordings are obtained by using white light passing the sample and recorded on a streak camera placed after a spectrometer (from Abrahamsson *et al.*[36]).

sensitizer quantification. The sensitizing agents can be seen as *optical contrast agents*. An illustration of such time-resolved, broadband absorption measurements of a sample containing water is given in Fig. 10.7.[36]

Here there is a parallel to efforts using laser-produced X-rays for enhanced imaging of conventional contrast agents, such as iodine or gadolinium, and to achieve sharp images using ballistic X-rays in a way similar to the techniques used for optical mammography discussed below (see, e.g., Grätz *et al.*[37] and Herrlin *et al.*[38]).

Holographic techniques have recently been developed using phase modulators. Spatial resolution of structures inside scattering media is achievable using such techniques.[39]

Optical techniques largely developed for biomedical applications have recently been put to work to assess the concentration of the active components of pharmaceutical preparations, such as tablets. White tablets are very strongly scattering, calling for time-resolved techniques, as discussed above, to allow a scatter-corrected measurement of true absorption and thus concentration.[40] Such techniques have also been applied to the study of fruits, wood etc.[41,42]

10.6.4 Optical mammography

Mammography using X-rays is now being pursued as a screening technique for early mammary malignancies. It is efficient, but a dose of ionizing radiation invariably also can induce cancer – especially in subjects carrying the ataxia-telangiectasia gene. There is a quest to reduce the dose, also through the use of gated viewing of laser-produced X-rays.[37] The use of ballistic photons, i.e. photons which are minimally deviated when passing tissue and selected on the criterion of a minimum passage time through the tissue, is one route pursued also in the optical regime (see, e.g., Andersson-Engels *et al.*[43] and Berg *et al.*[44]). Through gated viewing sharper images can be obtained. Tomographic inversion techniques in systems comprising multiple optical transmitters and detectors are used for assessment of optical anomalies, such as tumors. Also CW techniques, while having limited resolution, have been implemented.[45]

10.6.5 Photoacoustic spectroscopy

Photoacoustic detection uses the fact that absorbed light corresponds to a heating of the absorbing material. If the light is periodically switched on and off, an acoustic wave with an intensity proportional to the absorbed energy is generated. The great advantage of using photoacoustic detection in scattering media, such as human tissue, is that the acoustic wave is much less affected by scattering and absorption than optical radiation. On excitation, the light can be distributed diffusely, as naturally happens due to the strong scattering of optical radiation. However, the absorption and the origin of the acoustic waves are localized, and the messenger acoustic wave propagates without much scattering. In this way much sharper images can be generated, and the interrogation depth in tissue is much enhanced, since optical attenuation occurs only for the incident light. Since the absorption is governed by the wavelength of the laser light, a spectroscopic selectivity is obtained allowing, e.g., sharp imaging of blood vessels or areas marked with absorbers with contrast properties, e.g. in differential absorption studies.

Although the principles and advantages of photoacoustic detection were noted early on,[46] it is only more recently that the great advantages of such techniques have been realized. This is partly due to the fact that standard ultrasound imaging technology could be combined with photoacoustics, rendering optical absorption images of unprecedented quality. The spatial resolution is very high, making photoacoustic microscopy a very powerful tool. The exciting field of photoacoustic imaging is covered in several recent reviews (see, e.g., Oraevsky and Wang[47] and Wang[48]).

It is also possible to tag a particular site inside a scattering medium with a focused ultrasound beam. The sound waves induce a periodic movement of the molecules, and also a periodic change in the index of refraction. This gives rise to sidebands on the optical frequency. By heterodyne techniques, beating the

emerging light with a beam taken directly from the excitation laser, it is possible to isolate the light coming specifically from the tagged area. By scanning the focus of the ultrasound beam through the sample a sharp 3-D image can be obtained.[49]

10.6.6 Microscopy

Numerous techniques for optical microscopy have been developed.[50] Normally, contrast is generated because of absorption in the sample which is transilluminated. Staining and filtering techniques have enhanced the diagnostic performance of microscopy. A recent development is to take full advantage of the spectroscopic information using multispectral imaging. Normally, the spectroscopy is performed on the detection side, necessitating the use of expensive arrays of filters or a tuneable filter, e.g. of liquid crystal type. A different and cheaper approach is to use multiple LEDs with defined narrow-band emission characteristics as illumination sources which are activated sequentially[51] (see Fig. 10.8). All the image processing techniques well known from satellite imagery can then be used to extract useful information, e.g. the presence of malaria parasites in blood smears.

Also, in microscopy light scattering reduces the quality of the images obtained. As a remedy for this problem the technique of confocal microscopy[52] was developed. Using confocal small apertures for illumination and detection, out-of-focus scattering can be suppressed. Imaging can then be performed, layer by layer in thick targets.

10.6.7 Optical coherence tomography

Another very powerful technique to suppress blurring due to scattering is the optical coherence tomography (OCT) technique. The technique has a precursor in efforts to achieve high resolution in lidar-like measurements of the reflections from different layers in the eye. Pushing laser pulse-length down and increasing the temporal response of the detection system allowed different optical constituents of the eye to be identified.[53] However, it was realized that a much better lidar-like resolution could be obtained by using a broadband, CW source in a Michelson interferometer arrangement, in which constructive interference between light traveling the two arms of the interference is achieved for all colors only when the lengths of the arms are identical.[54,55] By scanning the length of the external arm mechanically, a depth scan through the scattering tissue is actually performed. Combined with fast lateral scanning of the beam, a high resolution in all three dimensions can be achieved. OCT techniques have now been developed to a very high degree of sophistication, and commercial equipment is now being used for various applications. Spectroscopic resolution can also be achieved. Interestingly, we note that femtosecond lasers are a preferred light source in OCT, not because of their short pulse lengths (see above) but because of their very large spectral coverage as a consequence of the ultrashort

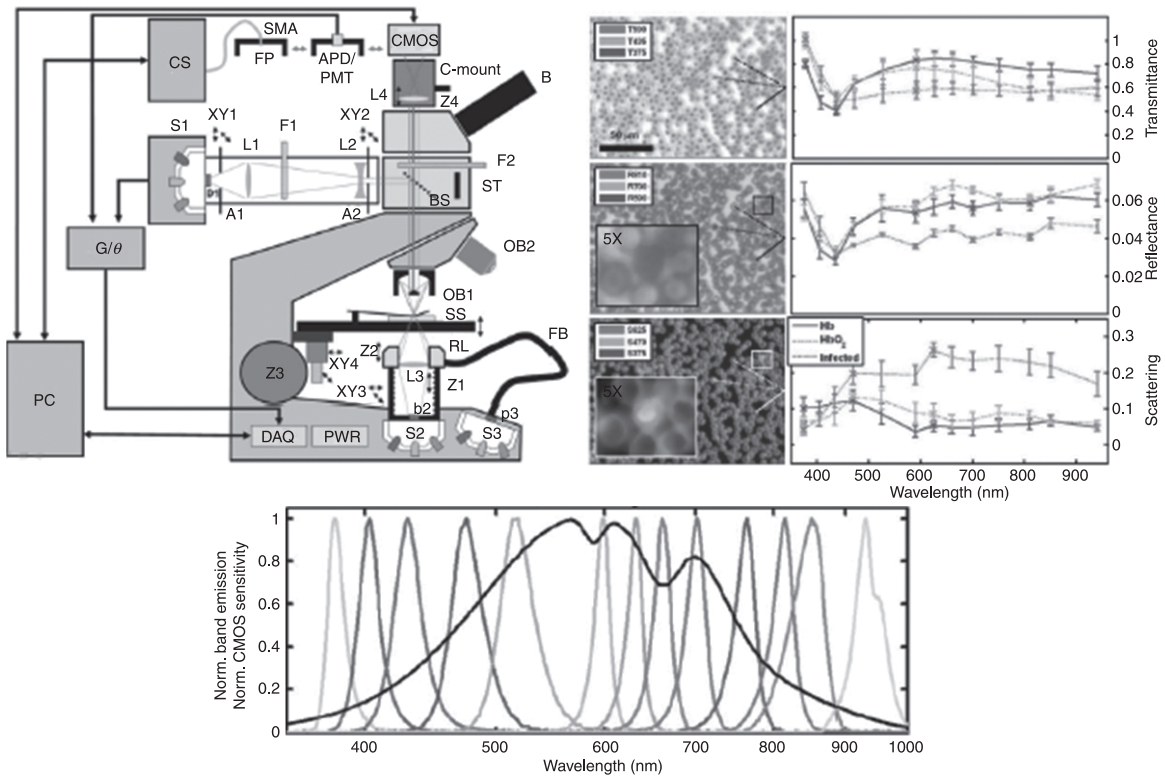

10.8 The use of light-emitting diodes (LEDs) for multispectral microscopy in transmission, reflectance and dark field illumination. Malaria detection is illustrated as an application (from Brydegaard *et al.*[51]).

pulse when subjected to Fourier transformation. Reviews of the OCT field can be found in Schmitt[56] and Drexler *et al.*[57]

Normally, OCT imaging is performed by scanning the spot of interrogation through the tissue. However, it is also possible to pursue OCT in a wide field mode, where a surface is illuminated and the interferograms are recorded in parallel on an imaging detector with a multitude of pixels.[58] The technique uses technology which is known from imaging Fourier transform spectroscopy (the SpectraCube concept) for recording reflectance or fluorescence spectra from a surface. By scanning the arm of the Michelson interferometer, interferograms are recorded from a swiftly read-out CCD detector.[59]

10.7 Fluorescence spectroscopy

The techniques discussed above mostly deal with the detection of absorbed radiation or the study of light, elastically scattered in the medium. We will now focus on optical radiation released in electric dipole transitions following the excitation in such processes. As discussed above, the emitted radiation is referred to as fluorescence and occurs red-shifted with regard to the excitation wavelength due to upper state radiation-less relaxation to the lowest vibrational level of the upper electronic state. Typical laser excitation wavelengths for inducing fluorescence (LIF) are 337 nm (nitrogen laser), 355 nm (frequency-tripled Nd:YAG laser) or 405 nm (diode laser tuned to the Soret band of porphyrins, which are frequently used as sensitizers for malignant tumors). The general behavior of LIF spectra has already been shown in Fig. 10.4.

10.7.1 Autofluorescence

Autofluorescence is used as a term for the fluorescence emitted by the normal constituents of tissue, such as amino acids, elastin, collagen, NADH, NAD^+, carotene, etc. Since the balance between such chromophores may be altered when normal tissue is transformed into malignant tumor, or when normal vessel wall is transformed into atherosclerotic plaque, autofluorescence can be useful in characterizing tissue for diagnostic purposes. It was noted early, for example, that the intensity in the blue spectral region is reduced in malignant tissue, a phenomenon likely ascribed to the transformation of strongly fluorescing NADH to weakly fluorescing NAD^+ associated with tumor development.[60] This phenomenon is evident also in Fig. 10.4.

Likewise, in the cardiovascular field, the difference in emission peak wavelength for elastin and collagen is of diagnostic value. In tissue with a lot of blood there will be a strong imprint of blood due to reabsorption of the fluorescence light. As is evident in Fig. 10.8, the Soret band of heme around 405 nm is very prominent. There are further absorption peaks at 540 and 580 nm, as already discussed in connection with surgical applications. Clearly, it is very important to take blood

reabsorption into account, either by modeling all chromophores in interaction or by evaluating ratios of intensities at wavelengths where the blood absorption is the same.[61]

10.7.2 Marker substances and fluorescence imaging

Frequently, sensitizers used in PDT of malignant tumors also exhibit useful fluorescence properties (having a sharp fluorescence peak and a reasonable fluorescence yield). Since the sensitizers are localized preferentially in tumors, such tissues can be identified by an increased sensitizer fluorescence. This phenomenon was already illustrated in Fig. 10.4, showing that, by choosing a suitable excitation wavelength, useful intensities can be obtained for the sensitizer as well as for the autofluorescence signals. By ratioing the sensitizer fluorescence (increasing in tumors) with the autofluorescence (decreasing in tumors) a useful contrast enhancement can be achieved.[62] A ratio is a simple example of a function which is dimensionless, i.e. a function the value of which is expressed without a unit (for example π, being the ratio of the circumference and the diameter of a circle). Such functions have the added virtue of being

- independent of geometry (i.e. angle of incidence or distance);
- independent of fluctuations in the illumination (temporal or spatial);
- independent of wavelength-neutral attenuations.

Basically, the shape of the spectral curve is probed, rather than its intensity. A ratio of the kind described above is an example of a contrast function. An optimized contrast function F, exhibiting maximal discrimination D (in terms of mean values of $F - A_m$ and B_m – being maximally separated in terms of the average standard deviations σ_A and σ_B) from spectral data pertaining to class A (i.e. tumor) and class B (i.e. surrounding normal tissue).

$$D = \frac{\left| A_m - B_m \right|}{\sqrt[2]{\sigma_A^2 + \sigma_B^2}} \qquad [10.4]$$

Then, a threshold T, placed between the certified classes A and B, can effectively separate the classes in an automatic way. Such discrimination can be made in more than one dimension in a higher-dimensional space featuring, e.g., multiple ratios.

These types of arguments can be generalized to encompass the full shapes of the spectral curves. Then the evaluation would be done using statistical mathematics of the multivariate type, expressing spectral shapes in a limited number of principal components.[63–67] Multivariate techniques make the whole process of discrimination basically automated, even if not as transparent as in terms of the simplistic argument made above.

While discrimination concepts as explained above can be used effectively to identify selected tissue types using fiber-optical point sensors of the types described, e.g., in Ek *et al.*,[13] Andersson-Engels *et al.*,[68] Gustafsson *et al.*,[69] and Klinteberg *et al.*,[70] medical doctors would prefer imaging devices, in which tumor tissue, for example, would be imaged in a suitable false color in real time. Many approaches to achieve multicolor fluorescence imaging have been proposed, as discussed, e.g., in Andersson-Engels *et al.*[71,72] In practice, the use of up to four wavelength bands frequently suffices.[73–75] Imaging fluorescence demarcation of tumor is illustrated in Fig. 10.9.[76]

Apart from sensitizers, which also have the PDT action, different types of fluorescing beacon molecules that bind to specific types of tissues have been developed, frequently being of functionalized antibody type.[77] A famous example is the green fluorescent protein (GFP), for which a Nobel prize was awarded.[78]

10.7.3 Up-converting nanoparticles

When using fluorescent markers there is a frequent wish to keep the concentrations as low as possible. Then the underlying autofluorescence level can be a problem, even if a small sensitizer peak sitting on a slowly varying autofluorescence background can be lifted off, also in fluorescence imaging systems. A way around this problem is to use stepwise excitation using longer-wavelength photons in each step, thus avoiding induction of autofluorescence in the tissue.[79,80] Step-wise excitation of suitable molecules follows the line long since developed in basic atomic physics (see, e.g., Svanberg *et al.*[81]). Since the transitions are step-wise dipole transitions rather than multiphoton ones, strong signals can be achieved

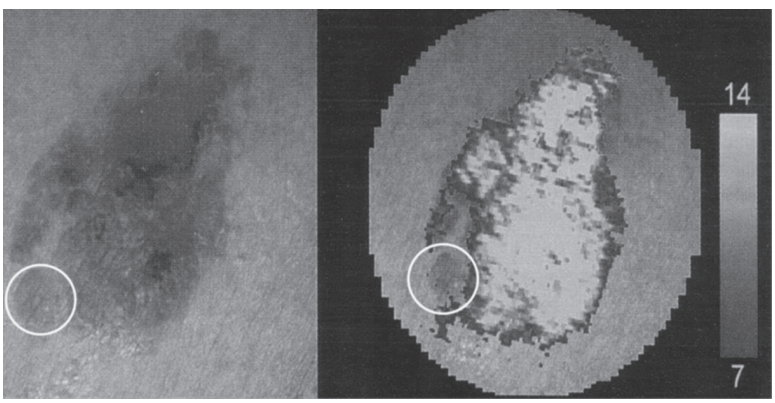

10.9 Illustration of LIF imaging demarcation of tissue. While most of the lesion image is basal cell carcinoma, a small part is actually benign nevus, as also indicated in the image (from Svanberg *et al.*[76]).

with moderate excitation densities. Suitable molecules are found among rare-earth compounds (frequently used as gain materials in lasers[82]), or in photon-echo quantum-information experiments,[83] which clearly cannot be used directly in the human body and do not have any targeting capability. Instead they are incorporated in nanoparticles, and suitable functionalization of the surface is intended to achieve beacon effects.[84]

Nanoparticles, especially made of gold, are also being investigated for thermal therapy of tumors. If functionalized with molecules targeting malignant cells, the nanoparticles can be localized preferentially to such cells and then thermally destroyed when the particles are heated using moderate fluxes of near-IR light which is strongly absorbed due to plasmonic resonances in the particles.[85]

10.7.4 Tomography in fluorescence diagnostics

In contrast to photoacoustic spectroscopy, the use of fluorescence markers of different types, as discussed above, is heavily influenced by scattering and absorption in the tissue. These types of problems occur on the detection side, not on the excitation side. Much effort has been invested in obtaining a high spatial resolution in the imaging of deep-lying lesions in tissue. Tomographic techniques, employed for slightly different reasons in, e.g., optical mammography (see Section 10.6.4), are helpful.[86] By shaping the phase field of the impinging light using a spatial light modulator (SLM) and using holographic techniques it has recently become possible to undo the detrimental effects of scattering and basically see clearly through tissue.[39]

10.7.5 Fluorescence lifetime spectroscopy and imaging

As discussed in Section 10.1, the temporal domain also presents substantial possibilities for discrimination and characterization of tissue types. Lifetimes of normal tissue constituents are of the order of 1 nanosecond, and thus systems with a high temporal resolution are needed. Since many sensitizing molecules, such as those containing porphyrins, have a substantially longer upper-state lifetime, it is possible to increase contrast in tumor localization by restricting the observation to later times after an abrupt excitation; afterglow detection.[87] Many molecules with similar time-integrated fluorescence signatures may have quite different lifetimes, enabling discrimination in the temporal domain. Actually, complex molecules building up tissue are frequently characterized by several decay times. In a study of constituents relating to vessel monitoring, the decay was fitted to three decay curves of different amplitude.[88] It was found that plaque discrimination from normal vessel wall can be based on quite different decay times for elastin and collagen, resulting in a substantially longer afterglow in collagen-containing diseased vessels (see Fig. 10.10).[88]

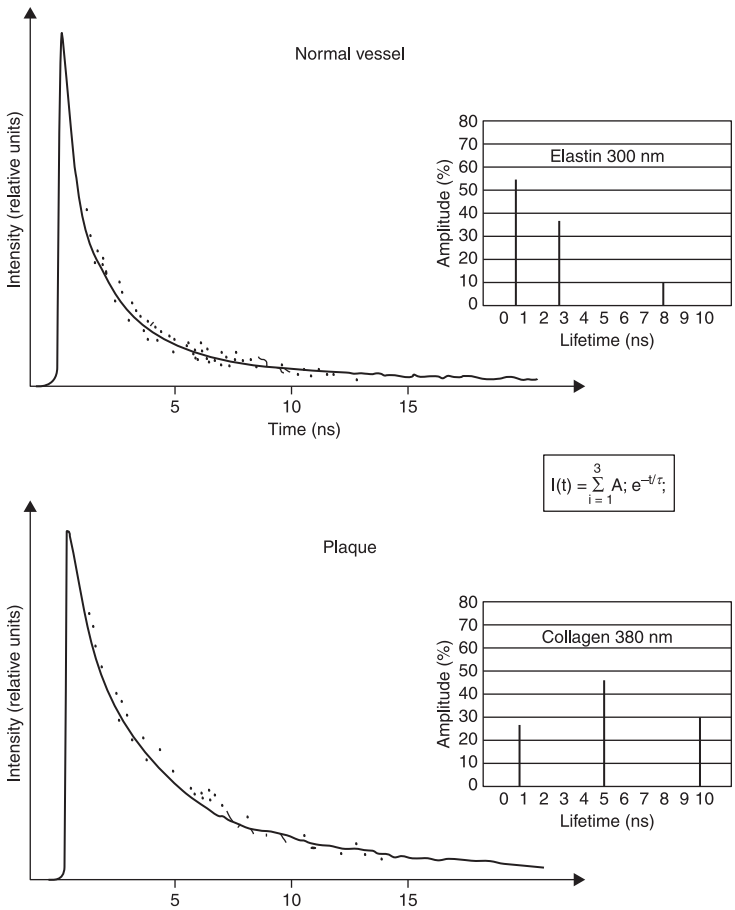

10.10 Different decay times for normal vessel wall and atherosclerotic plaque and lifetime components of elastin and collagen, suggesting a partial replacement of elastin with collagen in the disease (from Andersson-Engels *et al.*[88]).

A clinical system for lifetime imaging of skin areas is also available.[89] The technique is widely used in microscopy under the name of FLIM (*Fluorescence Lifetime Imaging*). Further information on FLIM can be found in Rück *et al.*[90] and van Munster and Gadella.[91]

10.7.6 Super-resolution microscopy techniques

The spatial resolution of a microscope is limited by the wave nature of light, and, according to the Abbe criterion, a resolution better than about half the wavelength cannot be achieved, i.e. about 300 nm in the visible region. That is the

reason why X-ray microscopy imaging techniques have been developed.[92] Another approach has been to use electrons, which, as discussed in Section 10.1, also have a wave nature, with wavelengths down to sub nm.[93,94] Resolution in the optical regime can be slightly improved by using two-photon absorption fluorescence spectroscopy.[95] Since the resulting intensity is quadratically dependent on the light intensity, most of the light comes from the area of highest intensity in a tightly focused beam. The effective focal spot then becomes smaller and resolution is improved.

Recently, the limitations of the Abbe criterion for resolution in the visible have been seriously challenged, and, in fact, several super-resolution techniques have been developed. The first of these techniques is Stimulated Emission Depletion (STED), which operates in fluorescence.[96,97] The light emanates from the primarily focused beam. However, by adding a donut-shaped beam which depletes the excited state due to stimulated emission, the fluorescence can be limited to the center of the donut, taking advantage of the non-linearity in the saturation process. In this way a spatial resolution down to about 20 nm has been achieved. Figure 10.11 illustrates the principles of STED. Similar non-linearities can be used in the frequency domain to achieve a spectral resolution below the natural radiation width limit.[99,100]

A further class of super-resolution methods rely on single-molecule fluorescence detection. Marker molecules attach to structures on the nm scale and give rise to fluorescence. The resulting light spot is again limited by the Abbe criterion. However, if the molecules are switchable from a bright and a dark state, and a given molecule can be made to emit many photons while the neighboring molecules do not emit, the center of the emission spot from a single molecule can be determined much more accurately than the position of an individual photon. The other molecules are later in turn switched on to emit. By plotting the center location of the molecules, a high spatial confinement, far below the diffraction

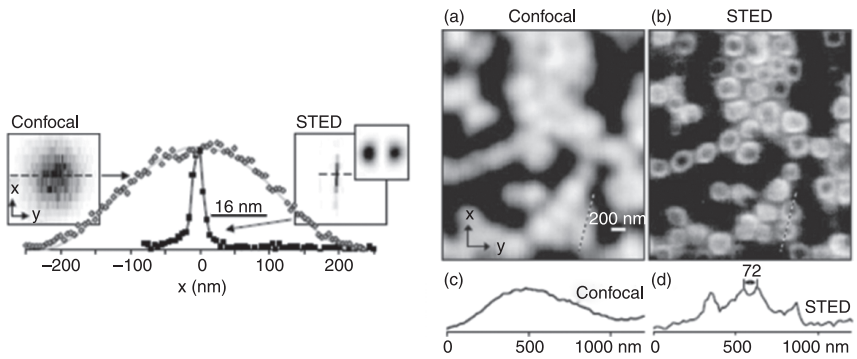

10.11 Principles of STED, resolution improvement, and illustration of images (from Westphal and Hell[98]).

limit, has been achieved. The technique is referred to as Stochastic Optical Reconstruction Microscopy (STORM);[101,102] a related technique is PALM (Photoactivated Localization Microscopy).[103]

10.8 Raman spectroscopy

Raman spectroscopy provides many possibilities for demarcation and imaging of particular constituents in tissue. As noted in Section 10.4.2, Raman signals correspond to vibrations in molecules. Specific groups are activated, such as C-H, C = O and CN, each having characteristic frequencies. A particular problem to be overcome is the need to suppress the very strong elastic signal which occurs close to the Raman peaks. This can be achieved with so-called notch filters, which help the spectrometer to observe weak signals on the shoulder of the prominent signals.

10.8.1 Spontaneous Raman spectroscopy

An example of spontaneous Raman signals of tissue is shown in Fig. 10.12, where sharp Raman signals are seen on a background of fluorescence.[104] Suppressing fluorescence is a major concern in Raman spectroscopy. Choosing long-wavelength driving lasers is one way to suppress fluorescence; however, this also reduces the intrinsic Raman intensity because of the $1/\lambda^4$ scattering cross-section dependence. Another approach is to use picosecond pulse excitation and detect signal only when the laser is on. In this way instant Raman scattering is retained while fluorescence with an afterglow on the ns scale is suppressed.[105]

10.8.2 Surface enhanced Raman spectroscopy (SERS)

Very strong enhancement of electromagnetic fields can be obtained using plasmonic resonances on the surface of particles, in particular silver or gold particles. Surface plasmons are charge oscillations along the surface of the particle. Sensitivity enhancements allowing Raman detection of even single molecules are possible.[106] Electromagnetic fields can be strongly modified in structures referred to as *metamaterials*, which are man-made materials tailored to feature plasmonic phenomena leading to new applications.

10.8.3 Second harmonic and coherent anti-Stokes Raman scattering (CARS) spectroscopy

In recent years several new non-linear optics phenomena have been used in developing new microscopy techniques. One such technique is second-harmonic generation in an anisotropic medium (i.e. muscle threads, nerves or other oriented structures, such as in elastin). The harmonic radiation is generated as a coherent beam. Images are generated by whisk-broom scanning the laser focal spot across the area to be imaged.

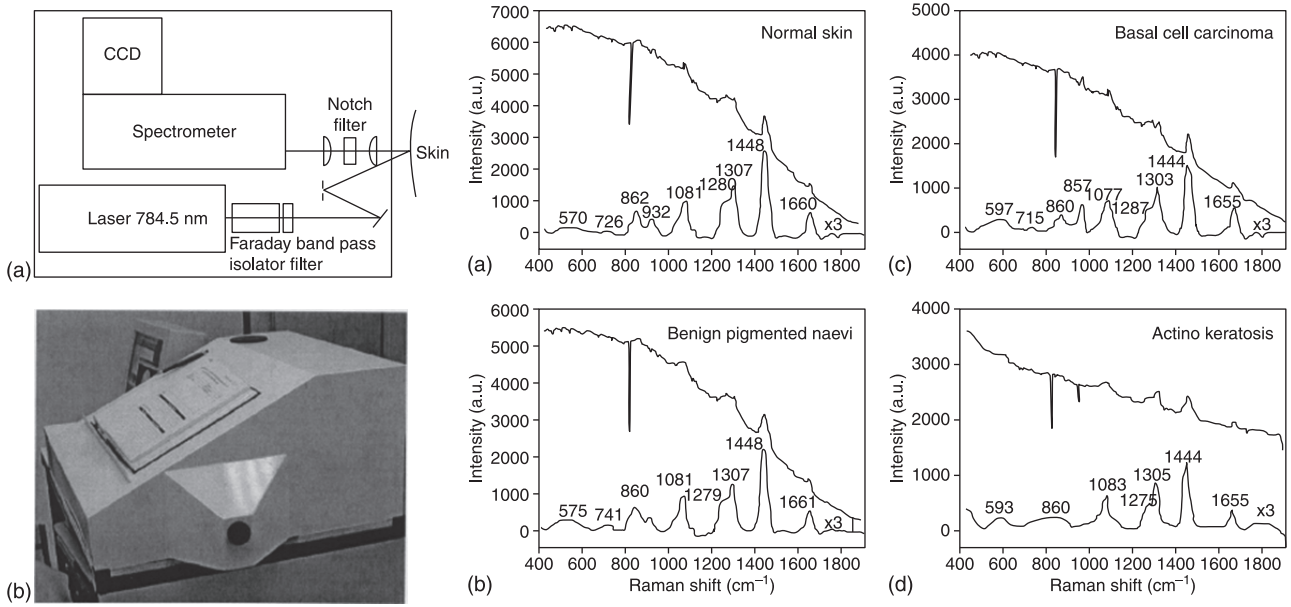

10.12 Clinical Raman spectrometer and examples of Raman spectra, superimposed on fluorescence, and lifted off the fluorescence signal, for different types of human skin (from Pålsson *et al.*[104]).

Coherent anti-Stokes Raman Scattering (CARS) generates images of molecules with specific molecular vibrational frequencies. Two laser beams, separated in frequency with the vibrational frequency to be probed, are used to generate a new coherent beam at the anti-Stokes frequency with regard to the laser, responsible for two of the driving fields in the coherent process (Section 10.3.2). CARS microscopy is becoming a powerful tool for biomedical microscopy.[107]

10.9 Gas in scattering media absorption spectroscopy (GASMAS)

10.9.1 Basic principles of GASMAS

Recently, a new method which monitors free gases in a scattering medium has been developed, combining techniques known from environmental trace gas detection with tissue optics as discussed above. The technique is denoted gas in scattering media absorption spectroscopy (GASMAS).[9] Many materials of organic origin, such as wood, polystyrene foams, fruit and other foods, as well as certain human structures, contain pores or cavities filled with free gas, such as oxygen, water vapor and carbon dioxide. Since the material is porous, by definition it gives rise to strong scattering (scattering occurs when there is a change in index of refraction). The key to the GASMAS technique is the observation that free gases have an absorptive linewidth which is typically 1000 to 10 000 times narrower than those typical for the solid or liquid host material. Using a tunable single-mode laser in combination with sensitive gas absorption techniques known from the environmental monitoring field, the imprint from the gas can be retrieved in the diffusely emerging light.[108] Figure 10.13 illustrates the GASMAS technique.

Polystyrene foam is a model material for exploratory measurements with the new technique.[109] Oxygen is a gas of particular interest, since it is ubiquitous and of utmost importance in, e.g., biomedicine. The oxygen A-band is located around 760 nm, where it is observed as a terrestrial Fraunhofer line in the sky radiation. The individual P- and R-branch lines have a pressure-broadened width of about 4 GHz (about 0.001 nm) at atmospheric pressure. Measured linewidths can be used for non-intrusive pressure assessment; likewise, the relative intensities of lines yield temperature information through the Boltzmann distribution. The lines are strongly forbidden, resulting in absorptive imprints of only a fraction of 1 percent for an ambient air pathlength of 1 m. Water vapor absorbs in a wide band around 980 nm; to avoid excessive attenuation of liquid water it is advantageous to operate around 935 nm. In a closed volume with free liquid water present it can be assumed that the relative humidity is 100 percent – then the concentration of the vapor is given by the temperature through the Arden-Buck relation. Since the wavelengths for oxygen and water vapor are quite close, the optical pathlength through the bulk medium will be similar and the water vapor

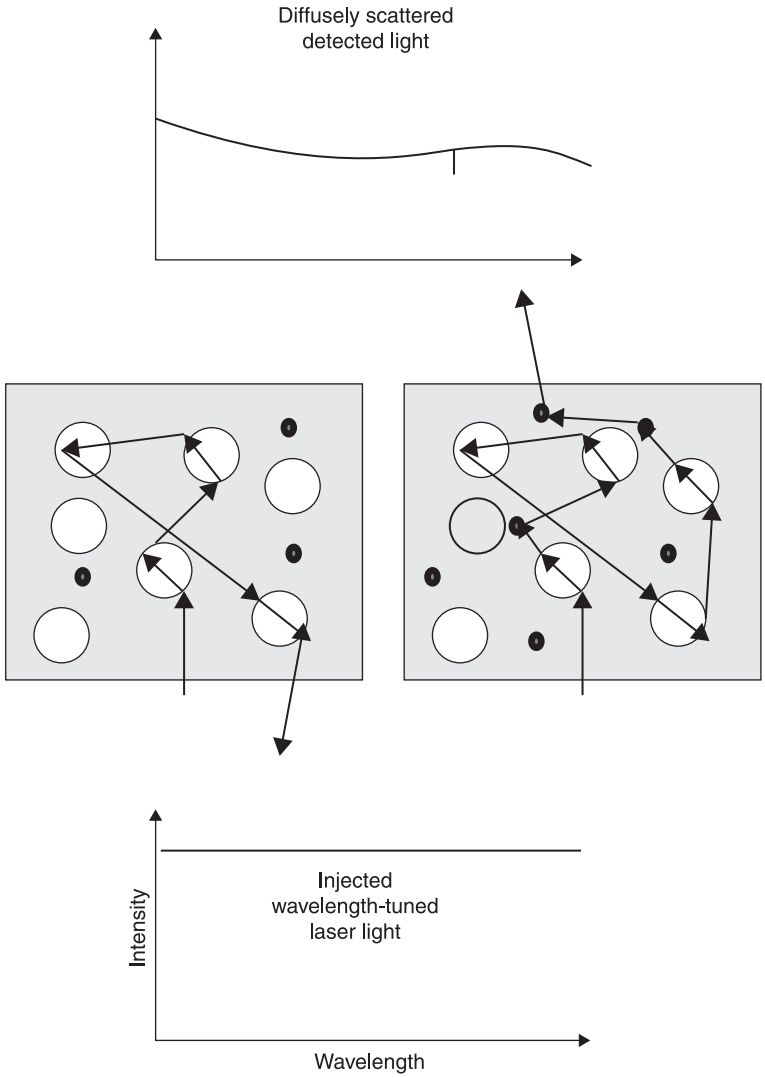

10.13 Basic principles for GASMAS recordings in porous materials.

signal can be utilized to eliminate this unknown quantity in assessments of oxygen concentration. Single-mode diode lasers of the distributed feedback (DFB) or vertical cavity surface emitting laser (VCSEL) types are useful sources of narrow-band radiation with output powers around 1 mW.

Other model materials are nanoporous ceramics, which have very strong scattering properties. In fact, it was recently shown that a 7 mm piece of ZrO_2 sintered ceramic exhibits an effective pathlength more than 700 times longer than

its physical size for light in transmission. With materials with fast gas exchange, miniature 'multipass' absorption cells without any precision optics to align can be accomplished.[110] When the pore sizes become comparable to or smaller than the mean free path length of the molecules, wall-collisional effects are observed, which can be useful for non-intrusive assessments of pore sizes.[108,111–113] We will now consider various applications of GASMAS related to biophotonics.

10.9.2 Food and pharmaceutical applications

Pharmaceutical tablets are porous and strongly scattering. They have been studied with broadband spectroscopy regarding non-intrusive assessment of the chemical composition, using time-resolved techniques with several individual pulsed diode-laser wavelengths or employing a femtosecond white-light source operating on self-phase modulation in, e.g., a photonic-bandgap fiber.[114] By monitoring oxygen gas signals using GASMAS, information on porosity can be obtained.[115]

Gas monitoring in food packages, e.g., in milk carton packages with a headspace, can readily be performed.[116] Now the cavity is a larger one, but still the multiple scattering brings us into the GASMAS regime. Normalizing to water vapor, the oxygen gas contents can be assessed – a parameter clearly related to freshness, etc. Frequently a modified atmosphere of nitrogen or carbon dioxide is used (modified atmosphere packaging, MAP) to increase shelf-life in a low-oxygen environment. The integrity of such packages can easily be assessed non-intrusively, revealing the actual status of the product rather than the date stamp information.[117,118] Also, bread and fruits have been studied by GASMAS.[116,119]

In addition to static gas measurements, the GASMAS technique can be used to study dynamic processes. When an object is subjected to an abrupt change in surrounding gas composition, the subsequent gas signal development gives information on diffusion processes. For example, samples of materials such as polystyrene foam or fruits can be placed overnight in a sealed plastic bag filled with nitrogen. After removal of the sample, the reinvasion of normal air, i.e. oxygen, can be studied.[109,116] As mentioned above, pressure can be assessed from the measured linewidth. This was utilized in studies of vacuum perforation processing of apples.[120]

10.9.3 ENT applications

Human sinus cavity disorders are very common and lead to the prescription of antibiotics in many cases when the problem is not actually of bacterial origin. Increasing bacterial resistance to antibiotics is a mounting global problem. A simple device allowing improved diagnostics of sinus cavities is of considerable interest. We have developed a method to illuminate the cavity from the skin and observe light emerging after having diffusely passed the cavity. For the maxillary (cheek) cavities a transmission or a reflection geometry can be chosen, while for

the frontal and maxillary cavities the light injection probe and the detector are placed on the same side but laterally displaced. Early work on healthy volunteers showed great promise for such a technique.[121,122] Oxygen and water vapor measurements are performed simultaneously by modulating the two laser sources at different frequencies for identification. The water vapor signal relates to the size of the gas-filled volume, while the ratio between the oxygen and the water vapor signals relates to the oxygen concentration. A clinical trial performed on 40 patients referred for CT skull radiography due to persistent sinus problems resulted in good correlation with the standard CT evaluation schemes for frontal and maxillary sinuses.[123] Also for the mastoideal bone, diagnostically useful information was obtained with the GASMAS technique.[124]

10.9.4 Neonatal children applications

Very recently, human GASMAS applications have been extended to the monitoring of lungs and intestines in newborn children. Lung function is the factor of paramount importance for prematurely born children, who, with proper care, can be saved even at a birth weight of 500 g (approximately 23rd week of pregnancy). Proof of principle measurements were performed on appropriately sized phantoms made out of boar lung covered with gelatin slabs prepared with scattering TiO_2 particles and absorbing ink to attain properties typical of human chest wall.[125] The concepts were verified in measurement on a newborn, full-term baby weighing 4 kg.[126] Water vapor is readily observed, and scaling suggests that it will also be possible to measure oxygen in premature children.

10.10 Conclusion and future trends

As illustrated in the present account, numerous spectroscopic techniques can be applied in biophotonics. Many techniques which have been developed for basic science are readily applicable in the medical field. In particular, many approaches used in the environmental field have their counterparts in the biomedical field, and vice versa. Actually, this observation has proved very useful, as noted, e.g., in Svanberg.[127] With the fast development of semiconductor lasers, fiber optics, compact spectrometers and computers, biophotonic applications of spectroscopy will have a growing impact in the field. The reliability and affordability of the techniques also imply that biomedical applications could become feasible in the Third World.[128–130]

10.11 Acknowledgements

The author gratefully acknowledges a most fruitful collaboration with numerous colleagues and students of physics and medicine during almost 30 years of joint research in laser medicine. This work has been supported by the Swedish Research

Council by direct grants and a Linnaeus grant to the Lund Laser Centre, the VINNOVA agency, the European Community, and the Knut and Alice Wallenberg Foundation.

10.12 References

1. S. Svanberg, *Atomic and Molecular Spectroscopy – Basic Aspects and Practical Applications*, 4th ed. (Springer, Heidelberg 2004).
2. A. Thorne, U. Litzén, and S. Johansson, *Spectrophysics* (Springer, Heidelberg 1999).
3. C.E. Banwell, and E.M. McCash, *Fundamentals of Molecular Spectroscopy* (McGraw-Hill, London 1994).
4. M.S. Albert, D.G. Cates, G. Driehuys, W. Happer, B. Saam, *et al.*, Biological magnetic resonance imaging using laser-polarized Xe-129. *Nature* **370**, 199 (1994).
5. M. Ebert, T. Grossmann, W. Heil, E.W. Otten, R. Surkau, *et al.*, MRI-imaging with hyperpolarized 3He, *Lancet* **347**, 9011 (1996).
6. B. Mazzolai, V. Mattoli, V. Raffa, G. Tripoli, P. Dario, *et al.*, A Multi-Disciplinary Approach to Study the Impact of Mercury Pollution on Human Health and Environment: The EMECAP Project, *RMZ – Materials and Geoenvironment* **51**, 682 (2004).
7. S. Svanberg, Geophysical Gas Monitoring using Optical Techniques: Volcanoes, Geothermal Fields and Mines, *Optics and Lasers in Engineering* **37**, 245 (2002).
8. R. Grönlund, M. Sjöholm, P. Weibring, H. Edner and S. Svanberg, Mercury Emissions from Chlor-Alkali Plants Measured by Lidar Techniques, *RMZ – Materials and Geoenvironment* **51**, 1585 (2004).
9. S. Svanberg, Gas in Scattering Media Absorption Spectroscopy – from Basic Studies to Biomedical Applications, *Lasers and Photonics Reviews*, Doi 10.1002/lpor.201200073 (2013).
10. C. Wang and P. Sahay, Breath Analysis Using Laser Spectroscopic Techniques: Breath Biomarkers, Spectral Fingerprints, and Detection Limits, *Sensors* **9**, 8230 (2009).
11. O. Svelto, *Principles of Lasers*, 5th ed. (Plenum, New York 2007).
12. J. Boulnois, Photophysical processes in recent medical laser developments: a review, *Lasers Med. Sci.* **1**, 47 (1986).
13. S. Ek, B. Anderson and S. Svanberg, Compact Fiber-Optic Fluorosensor Employing Light-Emitting Ultraviolet Diodes as Excitation Sources, *Spectrochim. Acta* B **63**, 349 (2008).
14. S. Andersson-Engels, A. Gustafsson, J. Johansson, U. Stenram and K. Svanberg, Laser-induced fluorescence used for localizing atherosclerotic lesions, *Lasers Med. Sci.* **4**, 171 (1989).
15. K.M. Morisseau and C.T. Rhodes, Pharmaceutical Uses of Near-Infrared Spectroscopy, *Drug Development and Industrial Pharmacy* **9**, 107 (1995).
16. M.S. Patterson, B. Chance and B.C. Wilson, Time-resolved reflectance and transmittance for the noninvasive measurement of tissue optical properties, *Appl. Opt.* **28**, 2331 (1989).
17. C. af Klinteberg, A. Pifferi, S. Andersson-Engels, R. Cubeddu and S. Svanberg, In vivo Absorption Spectroscopy of Tumor Sensitizers using Femtosecond White Light, *Appl. Opt.* **44**, 2213 (2005).
18. T.J. Farrell, M.S. Pattersson and B. Wilson, A diffusion theory model of spatially

resolved, steady-state diffuse reflectance for noninvasive determination of tissue optical properties *in vivo, Med. Phys.* **19**, 879 (1992).
19. J.R. Mourant, I.J. Bigio, D.A. Jack, T.M. Johnson and H.D. Miller, Measuring absorption coefficients in small volumes of highly scattering media: source-detector separations for which pathlengths do not depend on scattering properties, *Appl. Optics* **36**, 5655 (1997).
20. S. Svanberg, New developments in laser medicine, *Physica Scr.* **T72**, 69 (1997).
21. G. Pettit and R.W. Waynant, eds, *Lasers in Medicine* (Wiley, New York 1993).
22. T.J. Dougherty, C.J. Gomer, B.W. Henderson, G. Jori, D. Kessel, *et al.*, Photodynamic Therapy, *J. Nat. Cancer Inst.* **90**, 889 (1998).
23. J.C. Kennedy, R.H. Potter and D.C. Pross, Photodynamic Therapy with Endogenous Protoprophyrin IX: Basic Principles and Present Clinical Experience, *J. Photochem. Photobiol.* **6**, 143 (1990).
24. K. Svanberg, T. Andersson, D. Killander, I. Wang, U. Stenram, *et al.*, Photodynamic Therapy of Non-Melanoma Malignant Tumours of the Skin Utilizing Topical -Amino Levulinic Acid Sensitization and Laser Irradiation, *British J. of Dermatology* **130**, 743 (1994).
25. M. Tarstedt, I. Rosdahl, B. Berne, K. Svanberg and A.M. Wennberg, A randomized multicenter study to compare two treatment regimens of topical methyl aminolevulinate (Metvix)-PDT in actinic keratosis of the face and scalp. *Acta Derm. Venereol.* **85**, 424 (2005).
26. M. Soto-Thompson, A. Johansson, Th. Johansson, S. Andersson-Engels, S. Svanberg, *et al*., Clinical System for Interstitial Photodynamic Therapy with Combined On-line Dosimetry, *Appl. Optics* **44**, 4023 (2005).
27. J.J. Swartling, J. Axelsson, S. Svanberg, S. Andersson-Engels, K. Svanberg, *et al.*, System for Interstitial Photodynamic Therapy with On-line Dosimetry – First Clinical Experinces of Prostate Cancer, *J. Biomed. Optics* **15**, 058003 (2010).
28. N.C. Zeitouni, A.R. Oseroff, and S. Shieh, Photodynamic therapy for nonmelanoma skin cancers: Current review and update, *Molecular Immunology* **39**, 1133–1136 (2003).
29. Z. Huang, A review of progress in clinical photodynamic therapy, *Technology in Cancer Research & Treatment* **4**, 283–293 (2005).
30. J.P. Payne and J.P. Severinghaus, eds, *Pulse Oximetry* (Springer, Heidelberg 1986).
31. M. Lindén, H. Golster, S. Bertuglia, A. Colantuoni, F. Sjöberg, *et al.*, Evaluation of enhanced high-resolution laser Doppler imaging in an *in vitro* tube model with the aim of assessing blood flow in separate microvessels, **56**, 261–270 (1998).
32. A.M.K. Enejder, C. af Klinteberg, I. Wang, S. Andersson-Engels, N. Bendsoe, *et al.*, Blood Perfusion Studies on Basal Cell Carcinomas in Conjunction with Photodynamic- and Cryo Therapy Employing Laser-Doppler Imaging, *Acta Derm. Venereol.* **80**, 19 (2000).
33. E. Krite Svanberg, P. Wollmer, S. Andersson-Engels and J. Åkeson, Physiological influence of basic perturbations assessed by non-invasive optical techniques in humans. *Appl. Physiol. Nutr. Metab.* **36**, 946 (2011).
34. B.J. Chance, J.S. Leigh, H. Miyake, D.S. Smith, S. Nioka, *et al.*, Comparison of time-resolved and –unresolved measurements of deoxyhemoglobin in brain, *Proc. Natl. Acad. Sci. USA* **85**, 4971 (1988).
35. D.T. Delphy, M. Cope, P. van der Zee, S. Arridge, S. Wray, *et al.*, Estimation of optical pathlength through tissue from direct time of flight measurement, *Phys. Med. Biol.* **33**, 1433 (1988).

36. Ch. Abrahamsson, T. Svensson, S. Svanberg, S. Andersson-Engels, J. Johansson, *et al.*, Time and Wavelength Resolved Spectroscopy of Turbid Media Using Light Continuum Generated in a Crystal Fibre, *Optics Express* **12**, 4103 (2004).
37. M. Grätz, A. Pifferi, C.-G. Wahlström and S. Svanberg, Time-gated imaging in radiology: Theoretical and experimental studies, *IEEE Sel. Top. Quant. Electr.* **2**, 1041 (1996).
38. K. Herrlin, C. Tillman, M. Grätz, C. Olsson, H. Pettersson, *et al.*, Contrast-Enhanced Radiography by Differential Absorption Using a Laser-Produced X-ray Source, *Invest. Radiology* **32**, 306 (1997).
39. I.M. Vellekoop and A.P. Mosk, Phase control algorithms for focusing light through turbid media, *Opt. Comm.* **281**, 3071 (2008).
40. C. Abrahamsson, J. Johansson, S. Andersson-Engels, S. Svanberg and S. Folestad, Time-resolved NIR spectroscopy for quantitative analysis of intact pharmaceutical tablets, *Anal. Chem.* **77**, 1055 (2005).
41. R. Cubeddu, C. D'Andrea, A. Pifferi, P. Taroni, A. Torricelli, *et al.*, Nondestructive quantification of chemical and physical properties of fruits by time-resolved reflectance spectroscopy in the wavelength range 650–1000 nm, *Applied Optics* **40**, 538 (2001).
42. C. D'Andrea, A. Nevin, A. Farina, A. Bassi and R. Cubeddu, Assessment of variations in moisture content of wood using time-resolved diffuse optical spectroscopy, *Applied Optics* **48**, B87–B93 (2009).
43. S. Andersson-Engels, R. Berg, S. Svanberg and O. Jarlman, Time-resolved Transillumination for Medical Diagnostics, *Optics Letters* **15**, 1179 (1990).
44. R. Berg, O. Jarlman and S. Svanberg, Medical Transillumination Imaging Using Short-Pulse Diode Lasers, *Appl. Opt.* **32**, 574 (1993).
45. S.B. Colak, M.B. van der Mark, G.W. Hooft, J.H. Hoogenraad, E.S. van der Linden, *et al.*, Clinical optical tomography and NIR spectroscopy for breast cancer detection, *IEEE J. Sel. Top. Quantum Electron.* **5**, 1143 (1999).
46. A.A. Oraevsky, S.L. Jacques, R.O. Esenaliev, and F.K. Tittel, Time-Resolved Optoacoustic Imaging in Layered Biological Tissues, in: *Advances in Optical Imaging and Photon Migration*, ed. by R. R. Alfano, Academic Press, New York, vol. 21, pp. 161 (1994).
47. A.A. Oraevsky and L.V. Wang, *Photons plus Ultrasound: Imaging and Sensing* (SPIE, Bellingham, 2007) Vol. 643.
48. L.V. Wang, Prospects of Photoacoustic Tomography, *Med. Phys.* **35**, 5758 (2008).
49. F. Ramaz, B.C. Forget, M. Atlan, A.C. Boccara, M. Gross, *et al.*, Photorefractive detection of tagged photons in ultrasound modulated optical tomography of thick biological tissues, *Optics Express* **12**, 5474 (2004).
50. B. Herman and J.J. Lemasters, *Optical Microscopy – Emerging Methods and Applications* (Academic Press, Orlando 1993).
51. M. Brydegaard, A. Merdasa, H. Jayaweera, J. Ålebring and S. Svanberg, Multimode Imaging Spectrometer for Angular-Resolved Optical Diagnosis on the Micro-Scale, *Rev. Sci. Instr.* **82**, 123106 (2011).
52. R.H. Webb, Confocal optical microscopy. *Rep. Prog. Phys.* **59**, 427 (1996).
53. J.G. Fujimoto, S. DeSilvestri, E.P. Ippen, C.A. Puliafito, R. Margolis, *et al.*, Femtosecond optical ranging in biological systems, *Optics Lett.* **11**, 150 (1986).
54. D. Huang, E.A. Swanson, C.P. Lin, J.S. Schuman, G.W. Stinton, *et al.*, Optical coherence tomography. *Science* **254**, 1178 (1991).

55. W. Drexler, H. Sattmann, B. Hermann, T.H. Ko, M. Stur, *et al*., Enhanced visualization of macular pathology with the use of ultra-high resolution optical coherence tomography. *Arch. Ophthalmol.* **121**, 695 (2003).
56. J.M. Schmitt, Optical Coherence Tomography (OCT): A Review, *IEEE J. Sel. Top. Quant. Electr.* **5**, 1205 (1999).
57. W. Drexler, U. Morgner, R.K. Ghanta, F.X. Kärtner, J.S. Schuman, *et al.*, Ultrahigh-resolution ophthalmic optical coherence tomography, *Nature Medicine* **7**, 502 (2001).
58. A. Dubois, L. Vabre, A.C. Boccara and E. Beaurepaire, High-resolution full-field optical coherence tomography with a Linnik microscope, *Applied Optics* **41**, 805 (2002).
59. Z. Malik, D. Cabib, R.A. Buckwald, Y. Garini and D. Soenkeson, A novel spectral imaging system combining spectroscopy with imaging – Applications for biology. *SPIE* **2329**, 180 (1994).
60. K. Svanberg, E. Kjéllen, J. Ankerst, S. Montán, E. Sjöblom, *et al.*, Fluorescence Studies of Hematoporphyrin Derivative (HPD) in Normal and Malignant Rat Tissue, *Cancer Research* **46**, 3803 (1986).
61. S. Andersson-Engels, A. Gustafson, J. Johansson, U. Stenram, K. Svanberg, *et al.*, Laser-Induced Fluorescence used in Localizing Atherosclerotic Lesions, *Lasers in Medical Sciences* **4**, 171 (1989).
62. J. Ankerst, S. Montán, K. Svanberg and S. Svanberg, Laser-Induced Fluorescence Studies of Hematoporphyrin Derivative (HPD) in Normal and Tumor Tissue of Rat, *Appl. Spectr.* **38**, 890 (1984).
63. K. Esbensen, *Multivariate Data Analysis in Practice* (CAMO ASA, Oslo 2006).
64. L. Eriksson, E. Johansson, N. Kettaneh-Wold, J. Trygg, C. Wikström, *et al*., *Multi- and Megavariate Data Analysis, Part I: Basic Principles and Applications*, 2nd Ed. (Umetrics Academy, Umeå 2007).
65. L. Eriksson, E. Johansson, N. Kettaneh-Wold, J. Trygg, C. Wikström, *et al.*, *Multi- and Megavariate Data Analysis, Part II: Advanced Applications and Method Extensions*, 2nd Ed. (Umetrics Academy, Umeå 2007).
66. R.A. Johnson and D.W. Wichern, *Applied Multivariate Statistical Analysis*, 6th ed. (Prentice Hall 2007).
67. P. Weibring, T. Johansson, H. Edner, S. Svanberg, B. Sundnér, *et al.*, Fluorescence lidar imaging of historical monuments, *Applied Optics* **40**, 6111 (2001).
68. S. Andersson-Engels, J. Ankerst, J. Johansson, K. Svanberg and S. Svanberg, Tumour Marking Properties of Different Hematoporphyrins and Tetrasulphonated Phthalocyanine – a Comparison, *Lasers in Medical Sciences* **4**, 115 (1989).
69. U. Gustafsson, S. Pålsson and S. Svanberg, Compact Fiber-optic Fluorosensor using a Continuous-wave Violet Diode Laser, *Rev. Sci. Instr.* **71**, 3004 (2000).
70. C. af Klinteberg, M. Andreasson, O. Sandström, S. Andersson-Engels and S. Svanberg, Compact Medical Fluorosensor for Minimally Invasive Tissue Characterization, *Review of Scientific Instruments* **76**, 034303 (2005).
71. S. Andersson-Engels, C.A.F. Klinteberg, K. Svanberg and S. Svanberg, In vivo fluorescence imaging for tissue diagnostics, *Phys. Med. Biol.* **42**, 815 (1997).
72. S. Andersson-Engels, K. Svanberg and S. Svanberg, Fluorescence Imaging in Medical Diagnostics, Chapter 10 in J.G. Fujimoto and D.L. Farkas, *Biomedical Optical Imaging* (Oxford University Press, Oxford 2009) pp. 265–305.
73. S. Montán, K. Svanberg and S. Svanberg, Multi-Color Imaging and Contrast Enhancement in Cancer Tumor Localization Using Laser-Induced Fluorescence in Hematoporphyrin (HPD)-Bearing Tissue, *Opt. Lett.* **10**, 56 (1985).

74. P.S. Andersson, S. Montán and S. Svanberg, Multi-Spectral System for Medical Fluorescence Imaging, *IEEE J. Quant. Electr.* **QE-23**, 1798 (1987).
75. K. Svanberg, I. Wang, S. Colleen, I. Idvall, C. Ingvar, *et al.*, Clinical Multi-colour Fluorescence Imaging of Malignant Tumours – Initial Experience, *Acta Radiol.* **38**, 2 (1998).
76. K. Svanberg, S. Andersson-Engels and S. Svanberg, Private communication.
77. J.J. Li, R. Geyer and W.H. Tan, Using molecular beacons as a sensitive fluorescence assay for enzymatic cleavage of single-stranded DNA, *Nucleic Acids Res.* **28**, 52 (2000).
78. O. Shimomura, Discovery of Green Fluorescent Protein (GFP), *Angewandte Chemie International Edition* **48**, 5590 (2009).
79. S.F. Lim, R. Riehn, W.S. Ryu, N. Khanarian, C.K. Tung, *et al*., In vivo and scanning electron microscopy imaging of up-converting nanophosphors in Caenorhabditis elegans, *Nano Letters* **6**, 169 (2006).
80. P. Svenmarker, C.T. Xu and S. Andersson-Engels, Use of nonlinear upconverting nanoparticles provides increased spatial resolution in fluorescence diffuse imaging, *Optics Letters* **35**, 2789 (2010).
81. S. Svanberg, P. Tsekeris and W. Happer, Hyperfine- Structure Studies of Highly Excited D and F Levels in Alkali Atoms Using a CW Tunable Dye Laser, *Phys. Rev. Lett.* **30**, 817 (1973).
82. J.C. Krupa and N.A. Kulagin, *Physics of Laser Crystals* (Springer 2003).
83. J.H. Wesenberg, K. Mølmer, L. Rippe and S. Kröll, Scalable designs for quantum computing with rare-earth-ion-doped crystals, *Phys. Rev. A.* **75**, 012304 (2007).
84. N. Bogdan, E. Martín Rodríguez, F. Sanz-Rodríguez, M.C. Iglesias de la Cruz, Á. Juarranz, *et al.*, Bio-functionalization of ligand-free upconverting lanthanide doped nanoparticles for bio-imaging and cell targeting, *Nanoscale* **4**, 3647 (2012).
85. G. Guillaume and R. Quidant, Thermo-plasmonics: using metallic nanostructures as nano-sources of heat, *Laser Photonics Reviews* 1–17 (2012), DOI 10.1002/lpor.201200003.
86. A. Hielscher, Optical tomographic imaging of small animals, *Current Opin. Biotechn.* **16**, 79 (2005).
87. R. Cubeddu, A. Pifferi, P. Taroni, A. Torricelli, G. Valentini, *et al.*, Fluorescence Lifetime Imaging: An Application to the Detection of Skin Tumors, *IEEE JSTQE* **5**, 923 (1999).
88. S. Andersson-Engels, A. Gustafson, J. Johansson, U. Stenram, K. Svanberg, *et al.*, An Investigation of Possible Fluorophores in Human Atherosclerotic Plaque, *Lasers in the Life Sciences* **5**, 1 (1992).
89. A. Ehlers, I. Riemann, M. Stark and K. König, Multiphoton fluorescence lifetime imaging of human hair, *Micr. Res. Techn.* **70**, 154 (2008).
90. A. Rück, C.H. Hülshoff, I. Kinzler, W. Becker and R. Steiner, SLIM: A new method for molecular imaging. *Micr. Res. Techn.* **70**, 485 (2008).
91. E.B. van Munster and T.W. Gadella, Fluorescence lifetime imaging microscopy (FLIM), *Adv. Biochem. Eng. Biotechnol.* **95**, 143 (2005).
92. J. Thieme, G. Schmahl, D. Rudolph and E. Umbach (eds), *X-Ray Microscopy and Spectromicroscopy* (Springer, Berlin, Heidelberg 1998).
93. L. Reimer, *Scanning Electron Microscopy. Physics of Image Formation and Microanalysis.* 2nd ed. Springer Series in Optical Sciences Vol. 45 (Springer, Berlin, Heidelberg 1998).
94. L. Reimer, *Transmission Electron Microscopy. Physics of Image Formation and*

Microanalysis. 4th ed. Springer Series in Optical Sciences Vol. 36 (Springer, Berlin, Heidelberg 1997).
95. W. Denk, J. Strickler and W. Webb, Two-photon laser scanning fluorescence microscopy, *Science* **248**, 7 (1990).
96. S.W. Hell and J. Wichmann, Breaking the diffraction resolution limit by stimulated emission: Stimulated emission-depletion fluorescence microscopy, *Opt. Lett.* **19**, 780 (1994).
97. S. Hell, Far-field optical nanoscopy, *Science* **316**, 1153 (2007).
98. W. Westphal and S. Hell, Nanoscale resolution in the focal plane of an optical microscope, *Phys. Rev. Lett.* **94**, 143903 (2005).
99. S. Svanberg, G.Y. Yan, T.P. Duffey, W.M. Du, T.W. Hänsch, *et al.*, Saturation spectroscopy for optically thick atomic samples, *J. Opt. Soc. Amer.* **B4**, 462 (1987).
100. C. Luo, S. Kröll, L. Sturesson and S. Svanberg, The Observation of Strongly Sub-Homogeneous Linewidths using High Contrast Transmission Spectroscopy: Experiment and Theory, *Phys. Rev.* **A53**, 1 (1996).
101. M.J. Rust, M. Bates and X. Zhuang, *Nat. Meth.* **3**, 793 (2006).
102. B. Huang, W. Wang, M. Bates and X. Zhuang, Three-dimensional super-resolution imaging by stochastic optical reconstruction microscopy, *Science* **319**, 810 (2008).
103. E. Betzig, G.H. Patterson, R. Sougrat, O. Wolf Lindwasser, S. Olenych, *et al.*, Imaging Intracellular Fluorescent Proteins at Nanometer Resolution, Science **313**, 1642 (2006).
104. S. Pålsson, N. Bendsoe, K. Svanberg, S. Andersson-Engels and S. Svanberg, *NIR Raman Spectroscopy for in vivo Characterization of Skin Lesions*, presented in S. Pålsson, PhD Thesis, Lund Reports on Atomic Physics LRAP-295 (2003).
105. D.V. Martyshkin, R.C. Ahuja, A. Kudriavtsev and S.B. Mirov, Effective suppression of fluorescence light in Raman measurements using ultrafast time gated charge coupled device camera, *Rev. Sci. Instrum.* **75**, 630 (2004).
106. K. Kneipp, H. Kneipp, R. Manoharan, I. Itzkan, R.R. Dasari, *et al.*, Surface-enhanced Raman scattering (SERS)—a new tool for single molecule detection and identification, *Bioimaging* **6**, 104 (1998).
107. C. Brackmann, J.O. Dahlberg, N.E. Vrana, C. Lally, P. Gatenholm, *et al.*, Non-linear microscopy of smooth muscle cells in artificial extracellular matrices made of cellulose, *J Biophotonics* **5**, 404 (2012).
108. M. Sjöholm, G. Somesfalean, J. Alnis, S. Andersson-Engels and S. Svanberg, Analysis of Gas Dispersed in Scattering Solids and Liquids, *Opt. Lett.* **26**, 16 (2001).
109. G. Somesfalean, M. Sjöholm, J. Alnis, C. af Klinteberg, S. Andersson-Engels, *et al.*, Concentration measurement of gas imbedded in scattering media employing time and spatially resolved techniques, *Appl. Optics* **41**, 3538 (2002).
110. T. Svensson, E. Adolfsson, M. Lewander, C.T. Xu and S. Svanberg, Disordered, Strongly Scattering Porous Materials as Miniature Multi-pass Gas Cells, *Phys. Rev. Lett.* **107**, 143901 (2011).
111. T. Svenson and Z. Shen, Laser spectroscopy of gas confined in nanoporous materials, *Appl. Phys. Lett.* **96**, 021107 (2010).
112. T. Svensson, M. Lewander and S. Svanberg, Laser Absorption Spectroscopy of Water Vapor Confined in Nanoporous Alumina: Wall Collision Line Broadening and Gas Diffusion Dynamics, *Optics Express* **18**, 16460 (2010).
113. C.T. Xu, M. Lewander, S. Andersson-Engels, E. Adolfsson, T. Svensson, *et al.*, Wall Collision Line Broadening at Reduced Pressures: Towards Non-destructive Characterization of Nanoporous Materials, *Phys. Rev. A* **84**, 042705 (2011).

114. J. Johansson, S. Folestad, M. Josefson, A. Sparén, C. Abrahamsson, *et al.*, Time-Resolved NIR/VIS Spectroscopy for Analysis of Solids: Pharmaceutical Tablets, *Appl. Spectrosc.* **56**, 725 (2002).
115. T. Svensson, L. Persson, M. Andersson, S. Svanberg, S. Andersson-Engels, *et al.*, Noninvasive Characterization of Pharmaceutical Solids by Diode Laser Oxygen Spectroscopy, *Appl. Spectr.* **61**, 784 (2007).
116. M. Lewander, Z.G. Guan, L. Persson, A. Olsson and S. Svanberg, Food Monitoring Based on Diode Laser Gas Spectroscopy, *Appl. Phys. B* **93**, 619 (2008).
117. M. Lewander, T. Svensson, S. Svanberg and A. Olsson, Non Intrusive Measurements of Food and Packaging Quality, *Packaging Technology and Science* **24**, 271 (2011).
118. P. Lundin, L. Cocola, A. Olsson and S. Svanberg, Non-intrusive Headspace Gas Measurements by Laser Spectroscopy — Performance Validated by an Intrusive Reference Sensor, *J. Food Eng.* dx.doi.org/10.1016/j.jfoodeng.2012.03.008 (2012).
119. L. Persson, H. Gao, M. Sjöholm and S. Svanberg, Diode Laser Absorption Spectroscopy for Studies of Gas Exchange in Fruits, *Lasers Opt. Engineering* **44**, 687 (2006).
120. U. Tylewicz, P. Lundin, L. Cocola, P. Rocculi, S. Svanberg, *et al.*, Gas in Scattering Media Absorption Spectroscopy (GASMAS) Detected Persistent Vacuum in Apple Tissue After Vacuum Impregnation, *Food Biophysics* **10**, 1483-011-9239-7 (2011).
121. L. Persson, K. Svanberg and S. Svanberg, On the Potential for Human Sinus Cavity Diagnostics Using Diode Laser Gas Spectroscopy, *Appl. Phys. B* **82**, 313 (2006).
122. L. Persson, M. Andersson, M. Cassel-Engquist, K. Svanberg and S. Svanberg, Gas Monitoring in Human Sinuses using Tunable Diode Laser Spectroscopy, *J. Biomed. Optics* **12**, 5 (2007).
123. M. Lewander, S. Lindberg, T. Svensson, R. Siemund, K. Svanberg, *et al.*, Clinical Study Assessing Information on the Maxillary and Frontal Sinuses using Diode Laser Gas Spectroscopy, *Rhinology* **50**, 26 (2012).
124. S. Lindberg, M. Lewander, T. Svensson, R. Siemund, K. Svanberg, *et al.*, Method for Studying Gas Composition in the Human Mastoid using Laser Spectroscopy, *Annals of Otology, Rhinology & Laryngology* **121**, 217 (2012).
125. M. Lewander, A. Bruzelius, S. Svanberg, K. Svanberg and V. Fellman, Non-intrusive Gas Monitoring in Neonatal Lungs Using Diode Laser Spectroscopy, *J. Biomed. Opt.* **16**, 127002 (2011), DOI:10.1117/1.
126. P. Lundin, E. Krite Svanberg, L. Cocola, M. Lewander, S. Andersson-Engels, *et al.*, Non-Invasive Gas Monitoring in Newborn Infants using Diode Laser Absorption Spectroscopy: A Case Study, *Proc. SPIE* **8229** (Bellingham, WA) 2012.
127. S. Svanberg, Laser Based Diagnostics – from Cultural Heritage to Human Health, *Appl. Phys. B* **92**, 351 (2008).
128. S. Svanberg, Laser Spectroscopy in Development, *Europhysics News* **33** (March/April 2002), p. 52.
129. K. Svanberg and S. Svanberg, Biomedical Laser Physics in Optics in Development, *Europhysics News* **35**, 1 (2004).
130. M. Brydegaard and S. Svanberg, Multispectral Imaging in Development, *Europhysics News* **42/5**, 4–5 (2011).